ISSN 1211–8796

*Acta Mus. Moraviae, Sci. geol.*
XCV (2010): 2, 95–129, 2010

# PETROGRAPHY, MINERALOGY, GEOCHEMISTRY AND GENETIC ASPECTS OF THE LAHN-DILL TYPE DEPOSIT OF MALÝ DĚD (= LEITERBERG) IN THE DEVONIAN VRBNO GROUP (SILESICUM), CZECH REPUBLIC

PETROGRAFIE, MINERALOGIE, GEOCHEMIE A GENETICKÉ ASPEKTY LOŽISKA TYPU LAHN-DILL MALÝ DĚD (=LEITERBERG) V DEVONSKÉ VRBENSKÉ SKUPINĚ (SILESIKUM), ČESKÁ REPUBLIKA

ARNO MÜCKE[1*], BOHUSLAV FOJT[2], ZDENĚK DOLNÍČEK[3]

*Abstract*

Mücke, A., Fojt, B., Dolníček, Z. (2010): Petrography, mineralogy, geochemistry and genetic aspects of the Lahn-Dill type deposit of Malý Děd (= Leiterberg) in the Devonian Vrbno Group (Silesicum), Czech Republic. – Acta Mus. Moraviae, Sci. geol., 2, 95, 95–129.

*Petrografie, mineralogie, geochemie a genetické aspekty ložiska typu Lahn-Dill Malý Děd (= Leiterberg) v devonské vrbenské skupině (silesikum), Česká republika*

The Lahn-Dill type deposit of Malý Děd located in the Silesian domain is a part of the Devonian metasedimentary and metavolcanic cover rocks (Vrbno Group) that contain about 30 small Lahn-Dill type iron-ore occurrences. The Malý Děd deposit occurs in close association with muscovite-biotite gneiss of the Precambrian Desná Dome. The investigations involved detailed petrographic-petrological studies supported by whole-rock geochemical, mineral (amphibole, biotite, chlorite, carbonate, feldspar, magnetite and ilmenite) and fluid inclusion studies.

The following metamorphosed rocks were observed: chlorite-amphibole(-magnetite-ilmenite) schist originating from submarine intrusions of a basaltic volcanite. The schist consists predominantly of chamosite (chlorite group) and subordinately ferroanthophyllite/grunerite which are arranged in the crenulation-cleavage texture. Other rock constituents, totally not higher than 20 vol. % are magnetite, ilmenite, graphite, albite, quartz and relics of ferrotschermakite. The other rocks are inhomogeneous and consist of layer-arranged mineral assemblages consisting of: (I) magnetite (mostly higher than 50 vol. %), chamosite, ferroanthophyllite/grunerite, rarely biotite and quartz; and (II) ankerite-dolomite solid solutions and calcite. Between (I) and (II) various transitions occur.

The basaltic volcanite is the source of the Lahn-Dill type iron-mineralization. The parental material of the assemblages (I) and (II) and mixtures of (I) + (II) (= III), identical with the ore body, was derived from iron-rich carbonates that precipitated from submarine volcanogenic exhalations. These precipitations were admixed with pyroclastic material of the basaltic volcanic activity. During the Variscan orogeny, the parental material of the ore body and the basaltic volcanite underwent metamorphic changes lying just at the border between low-grade to high-grade greenschist-facies conditions. The temperatures estimated from the system $CaCO_3$-$FeCO_3$ lie close to 450 °C, from the chlorite compositional geothermometer lying on average between 403 °C and 419 °C and from early "peak" $CO_2$-$H_2O$ fluid inclusions leading to ~ 450 °C (and ~ 3.5 kbars), fit well to the established conditions of our petrological investigations. The metamorphic overprint led to the formation and/or recrystallization of amphibole (in the form of felty aggregates consisting of tiny ferroanthophyllite/grunerite crystals), rarely biotite (siderophyllite), chamosite, magnetite, quartz, albite, calcite and ankerite-dolomite solid solutions which occur in varying proportions within the magnetite-rich ore body and the carbonate-free chlorite-amphibole(-magnetite-ilmenite) schist. In addition, multiple late-metamorphic to post-metamorphic fluid events have been distinguished in secondary fluid inclusions, characterized by contrasting compositions ($H_2O$-$CO_2$, pure aqueous, methane).

Of particular significance are ankerite-dolomite solid solutions that contain up to 85 mol. % ankerite-endmember. Such high concentrations were reported for the first time. Hitherto known ankerite concentrations do not exceed 70 mol. % in solid solution with dolomite.

*Key words:* Vrbno Group, Silesicum, Lahn-Dill type iron mineralization, petrography-petrology, fluid inclusions, microscopy, mineral chemistry, ankerite-dolomite solid solution, whole-rock geochemistry, genesis.

[1] Experimentelle und Angewandte Mineralogie, Göttinger Zentrum Geowissenschaften, Georg-August Universität, Goldschmidtstrass 1, 37077 Göttingen, Germany; arhemucke@gmx.de

[2] Institute of Geological Sciences, Masaryk University, Kotlářská 2, 611 37 Brno, Czech Republic; fojt@sci.muni.cz

[3] Department of Geology, Palacký University, Tř. 17. listopadu 12, 771 46 Olomouc, Czech Republic; dolnicek@prfnw.upol.cz

* Corresponding author

## 1. Introduction

The Devonian iron ores of the Lahn-Dill type are distributed from the eastern part of the Rheinisches Schiefergebirge via the Harz Mountains up to the Eastern Sudetes, middle Moravia and the Czech Silesicum. Kretschmer (1906, 1917 and 1918) was the first who described some of the Silesian deposits and correlated them to the iron mineralizations of the Lahn-Dill area (Rheinisches Schiefergebirge, Germany). The Silesian iron ores belong to the upper allochthonous sub-unit of the Desná Dome known as the Vrbno Group. The studied Malý Děd iron ore deposit represents a metamorphosed example of this type of mineralization in the Vrbno Group.

The genesis of Malý Děd was firstly discussed by Wilschowitz (1926). He described the wall rocks as metamorphosed limestones of Devonian age that were partially replaced by ore mineralization originating from ascending iron-rich solutions. Bederke (1938) had a similar opinion. However, Sellner (1930) and Pouba and Hettler (1950) correlated the Malý Děd mineralization with the chlorite-rich iron deposit of Mnišské jámy lying within the gneisses of the Desná Dome. Fojt *et al.* (1961 and 1993) and Fišera *et al.* (1982) explain the origin of the iron mineralizations by submarine exhalations and Skácel (1966) by postvolcanic exhalations followed by hydrotherms which became enriched in iron when percolating volcanic rocks.

Our paper presents data indicating that the iron-rich rocks of Malý Děd originated from carbonate precipitation of submarine-volcanogenic exhalations that were admixed with pyroclastic material of the basaltic volcanism.

## 2. Geological setting

The Malý Děd iron mineralization lies within the Silesian domain that consists apart from the Orlica-Snieznik Complex, the Velké Vrbno Unit, the Staré Město Unit and the Keprník Nappe of the Desná Dome and the Devonian metasedimentary/metavolcanic cover rocks (Vrbno Group) (Fig. 1). Some of these units/complexes or parts of them (e.g. the eastern and western parts of the Silesicum) are constituents of the Brunovistulian terrane. Therefore, the Silesicum represents for the most part metamorphosed equivalents of the Brunovistulicum which were incorporated in the Moravo-Silesian shear zone (Kalvoda *et al.* 2008), which is a NE-SW trending belt and at least 300 km long and in maximum 50 km in width. In Devonian, the tectonic evolution in the northern part of this belt (= northern Silesian domain) is characterized by rifting of continental crust with the development of a sub-parallel syn-rift basin (Moravo-Silesian Basin). In this basin, the later Devonian (Emsian to Givetian) stratigraphy is represented by a sequence of syn-rift sediments and

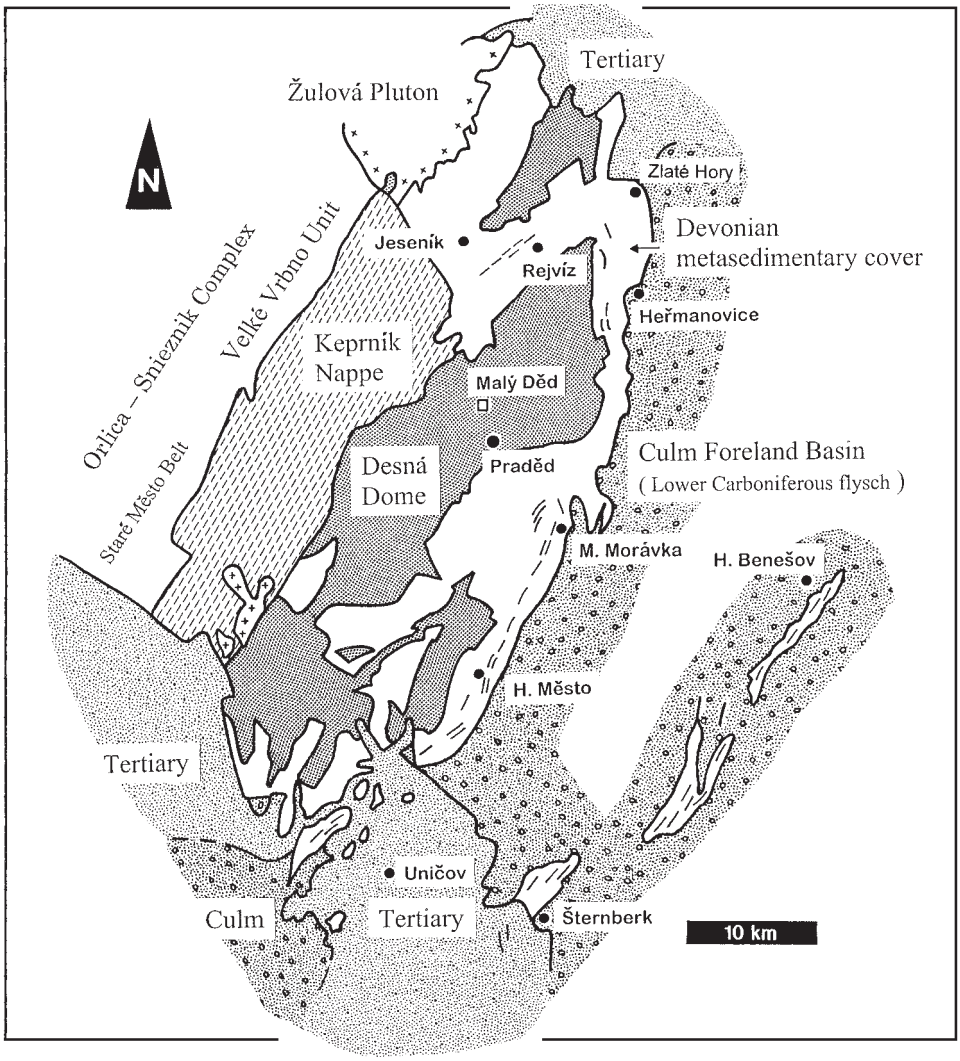


Fig. 1. Simplified geological map of the Silesian domain (High Jeseníky Mountains) after SCHULMANN and GAYER (2000) including the areas (indicated by small strokes) in which the Lahn-Dill type deposits are located and embedded within the Devonian metasedimentary cover rocks (Vrbno Group) according to SKÁCEL (1966 and 1987) and AICHLER *et al.* (1995).

volcanics (and post-rift carbonates) which have been affected by two major Variscan metamorphic events $M_2$ and $M_3$ (SCHULMANN and GAYER 2000). These led to the formation of metasediments and metavolcanics which are the main constituents of the Vrbno Group.

POUBA (1971), PETRÁNEK (1976), SKÁCEL (1987) and AICHLER *et al.* (1995) attributed the iron mineralizations to the first stage of the Variscan metallogeny with the formation of small Lahn-Dill type deposits which are related to submarine mafic volcanism. Except of PETRÁNEK (1976), these authors also presented maps showing the distribution of at least 30 iron-bearing areas within the Vrbno Group and the Šternberk-Horní Benešov Belt (Fig. 1) which both contain some stratabound Fe-Pb-Zn+Cu+Au sulphide deposits (Zlaté

Hory, Horní Město, Oskava and Horní Benešov; Fig. 1). The stratabound deposits are associated with felsic volcanism and genetically similar to the Rammelsberg deposit (Aichler *et al.* 1995) belonging to the so-called sediment-hosted massive sulphide deposits (Sawkins 1990). Although the Lahn-Dill type and the sulphide deposits are hosted by the same geological unit they never occur in one deposit (Pouba 1971).

Another type of iron-rich rocks, occurring at more than 10 localities (e. g. Sylvani, Kosaře, Švagrov, Zadní Hutisko and Mnišské jámy) are located within the same area, but are hosted within biotite-chlorite gneisses of the Desná Dome. The magnetite-rich rocks occur within, or close to, the basic Sobotín Massif, in an area of about 32 km$^2$. Pouba (1970) correlated them to banded iron-formations characterized by him as Sydvaranger type. However, according to recent investigations of Mücke and Losos (2007), the magnetite-rich rocks could have emplaced as apophyses originating from the mafic Sobotín Massif and are thus of magmatic origin.

## 3. Geological setting of Malý Děd deposit

In the southern part, the rocks of the Desná Dome are extensively overlain by metasedimentary and metavolcanic cover rocks of the Devonian Vrbno Group (Fig. 1). However, in other parts of the Desná Dome the outcrops of Devonian rocks are distinctly subordinate. This is the situation at Malý Děd deposit lying close to the Švýcárna cottage in an altitude of 1 270 m where Quaternary cover and Devonian rocks of the Vrbno Group occur in association with fine-grained gneiss (= metaarkose), muscovite-biotite gneiss and to lesser extent amphibolite belonging to the Precambrian Desná Dome (Fig. 2). GPS coordinates of the locality are 50°6'31.65"N, 17°12'53.95"E.

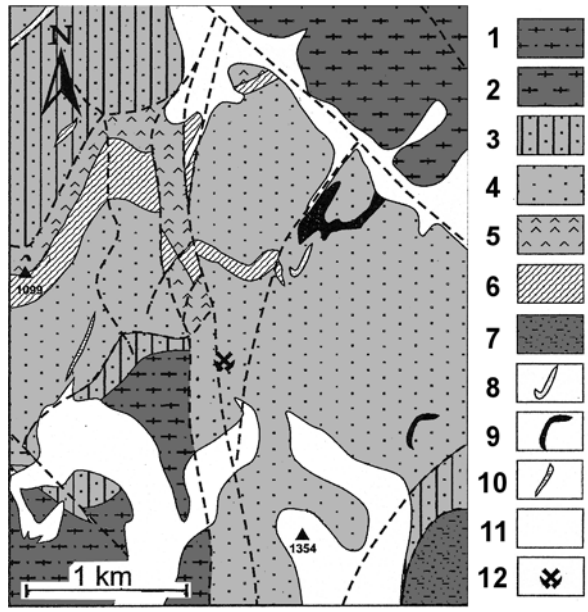


Fig. 2. Geological sketch of the studied area including the location of Malý Děd (Leiterberg) and the mountains of Malý Děd (1 354 m) and Malý Klín (1 099 m) (after Fišera *et al.*, 1982). Explanations: 1 – gneiss; 2 – mylonite; 3 – graphite-phyllite; 4 – muscovite-plagioclase phyllite; 5 – porphyroide; 6 – amphibolite; 7 – metaarkose; 8 – quartzite; 9 – green schists; 10 – metagabbro; 11 – Quaternary; 12 – location of the Malý Děd iron occurrence. (1, 2 and 7 = Desná Dome; 3, 4, 5, 6, 8, 9 and 10 = Vrbno Group).

During geodetical mapping in 1926, Roth discovered the iron mineralization of Malý Děd and WILSCHOWITZ (1929) mentioned the locality for the first time. The iron mineralization of Malý Děd forms a flat lensoidal body stretching NW-SE and dipping gently (about 20°) in SE-direction. The thickness of the ore body is about 3 m, exceptionally up to 5 m, and the average iron content is about 40 wt. %. The ore body which is closely associated with chlorite schist and limited by the wall-rock feldspar-graphite phyllite, was tracked down to a depth of 35 m (POUBA and HETTLER, 1950; FIŠERA *et al.*, 1982; FOJT *et al.*, 1993). Other wall-rocks described by FOJT *et al.* (1993) are muscovite-phyllite, marble and quartzite. The same authors recognized two textural types of ore mineralization which are either compact or occur in the form of weakly and irregularly developed bands and disseminated aggregates. The major ore mineral is magnetite. In lower amounts following minerals were detected: pyrrhotite, ilmenite, pyrite, chalcopyrite, iron-rich chlorite, ankerite, calcite, siderite and quartz.

## 4. Methods

### 4.1. Whole-rock analyses

In total 10 rock samples were analyzed by PHILLIPS PW 1480 XRF at the Georg-August-University of Göttingen. International standards were used for calibration (published in: Geostandard Newsletters, Vol. XIII, Special Issue, 1989). The XRF analyses were augmented by the determination of $H_2O^-$ (heating at 110 °C) and the loss on ignition (LOI) (heating at 1 000 °C). The $Fe^{2+}$ was determined by oxidimetric titration using of $KMnO_4$ (HEINRICH and HERRMANN 1990).

### 4.2. REE analyses

Eight whole-rock samples were selected for REE analyses carried out at the Georg-August-University of Göttingen by Perkin-Elmer SCIEX (Concorde, Ontario, Canada) ELAN DRC II ICP-MS spectrometer. Dissolution of rock powder was carried out by stepwise attack with HF, $HClO_4$ and $HNO_3$ at 180 °C for about 12 hours. All samples were normalized using international standardization by Ge, Rh, In and Re. Reproducibility was better than 1–2 %, accuracy was checked by comparison with international Standard JA-2 [GSJ Geochemical Reference samples: National Institute of Advanced Industrial Science and Technology (AIST)] and did not exceed 10–15 % deviation. All REE were corrected for Ba, REE plus oxygen isobaric interferences especially on $^{151}Eu$ by $^{135}Ba^{16}O$ and $^{157}Gd$ by $^{141}Pr^{16}O$.

### 4.3. Fluid inclusions

Fluid inclusions (FI) have been studied petrographically and microthermometrically in standard doubly-polished wafers. Recognition of individual genetic types of FI was made according to criteria described in literature (ROEDDER 1984, SHEPHERD *et al.* 1985, TOURET 2001). Microthermometric parameters were obtained using Linkam THMSG 600 heating-freezing stage mounted on Olympus BX-51 microscope. The stage was calibrated using inorganic standards and fluid inclusions with known temperatures of phase transitions. In $H_2O$-$CO_2$ inclusions, the following parameters have been measured: partial homogenization of $CO_2$ phase (Th-$CO_2$), melting temperature of $CO_2$ (Tm-$CO_2$), melting temperature of clathrate (Tm-cla) and temperature of total homogenization (Th-tot). For aqueous inclusions, the homogenization temperatures (Th), eutectic temperature (Te) and melting temperature of last ice (Tm-ice) were obtained. The interpretation of microthermometric data of $H_2O$-$CO_2$ and methane FI (composition, isochores) was performed using the Flincor software (BROWN 1989) with calibration by BOWERS and HELGESON (1983) and HOLLOWAY (1981), respectively. Salinity of aqueous inclusions was calculated according to BODNAR (1993), the isochores according to ZHANG and FRANTZ (1987).

### 4.4. Electron-microprobe analyses

Electron-microprobe analyses were carried out at the Institut für Endlagerforschung of the Technische Universität of Clausthal-Zellerfeld. Wavelenght-dispersive microprobe analyses were performed using CAMECA SX 100 instrument equipped with five WDS detectors. For quantitative measurement, 15 kV acceleration voltage, 20 nA current on the Faraday cup and 5 μm defocused beam were chosen. Counting times ranged between 12 and 22 s on the peak and total background analysing the X-ray Kα signals of Na, Mg, Al, Si, K, Ca, Ti, Mn and Fe. The PAP matrix correction method for the raw counts was employed (POUCHOU and PICHOIR 1984). The following standards were used for the analyses: kaersutite (Na, Mg, Al, Si, K, Ca), $TiO_2$ (Ti), alabandine (Mn) and hematite (Fe).

### 4.5. Calculation of mineral-formulae

The *amphibole* analyses were calculated as proposed by SCHUMACHER (1997) and classified following LEAKE *et al.* (1997). According to Schumacher's calculation scheme, the $Fe^{3+}$-values were averaged and calculated on the basis of electron neutrality for the formulae. $H_2O$ was calculated.

*Chlorite* analyses were calculated on the basis of 10 cations including minor $Ca^{2+}$, $Na^+$ and $K^+$. Two cases occur in the procedure of electron neutrality calculation for the chlorite formula $(Fe^{2+}, Mg, Fe^{3+}, Al)_6[OH)_8/(Si, Al)_4O_{10}]$:

1. The sum of the valences of the anions (= 28) is higher than the sum of the valences of the cations (under the assumption that iron is exclusively $Fe^{2+}$). The excess of negative charge is compensated by the introduction of a certain amount of $Fe^{3+}$.
2. The sum of the valences of the anions (= 28) is lower than the total of the valences of the cations (under the assumption that iron is exclusively $Fe^{2+}$). The deficiency of negative charges is compensated by the introduction of $O^{2-}$ instead of $OH^-$. As a consequence, $Fe^{3+}$ does not occur.

## 5. Sampling and sample description

During the years between 1995 and 2005 about 20 samples were collected from stockpiled material within the area of the former Malý Děd mine. Therefore, we could not obtain data on the distribution and abundance of the various ore types, shapes of their bodies and thicknesses as well as the geological relationship between each other. For this reason the study focused on petrographic and mineralogical description of 15 polished sections and 20 polished or covered thin sections, and petrological interpretations of data. Apart from the fluid inclusions studies, material of older collections was not used in this study.

The ores are fine-grained, compact, mostly dark and often greenish. Apart from chlorite, magnetite and pyrrhotite, the other constituents and the patterns are not macroscopically visible. Four ore assemblages types (I–IV) were recognized differing in the abundance of their major minerals.

**Type I**. The carbonate-bearing magnetite-chlorite/amphibole-quartz assemblage is the most abundant. The weakly developed layering and the varying abundance of quartz are characteristic (compare Figs. 3 and 4). The amount of quartz increases with decreasing chlorite/amphibole content (compare layer C with layer A of Fig. 3; and layer B with layer A of Fig. 4). Generally, quartz is interlayered with the other minerals (Fig. 3), but may also be irregularly distributed (Fig. 4). A minor constituent is carbonate which does not exceed 5 vol. %. and forms lensoidal polycrystalline aggregates (Fig. 3, layer A).

**Type II**. The carbonate-dominated (on average more than 80 vol. %) assemblage contains subordinate magnetite and rarely chlorite/amphibole and quartz in varying propor-

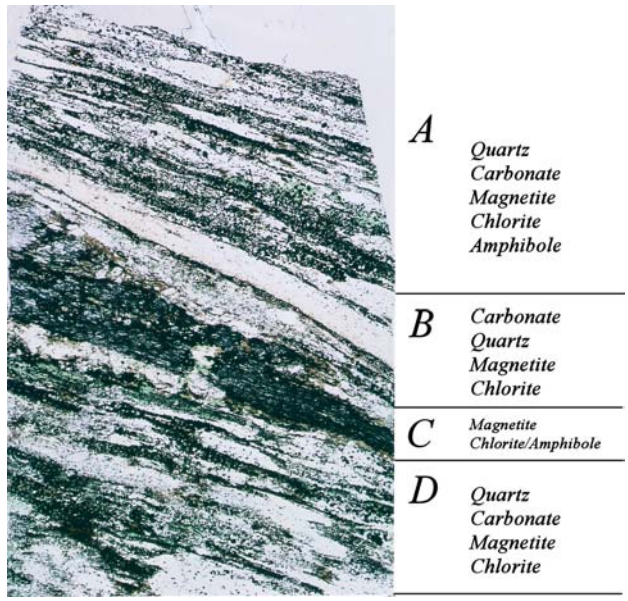


Fig. 3. Carbonate-bearing magnetite-chlorite/amphibole-quartz assemblage type I (sample 861/7) containing magnetite-rich layers (black) that are associated with chlorite, quartz, carbonate and amphibole (sublayers A to D). Note the occurrence of quartz in the form of layers (B) or in irregular distribution (A and D). Carbonate occurs often in the form of lensoidal bodies (A and D). One sublayer (C) consists predominantly of magnetite and chlorite/amphibole alone. Transmitted light, 4.5×2.5 cm.

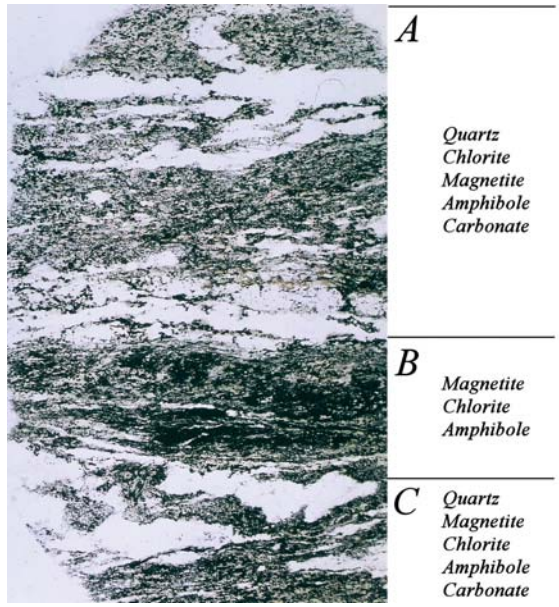


Fig. 4. Carbonate-bearing magnetite-chlorite/amphibole-quartz assemblage type I (sample 861/1) containing finely distributed magnetite (black) that is associated with chlorite, carbonate and amphibole (sublayers A to C). Due to the appearance of fine-grained magnetite, layering is less pronounced than in the samples of Fig. 3. Note the irregular distribution and shape of quartz. Transmitted light, 4.5×2.5 cm.

tions (5–20 vol. %). Layering becomes obvious in parts with abundant magnetite. The carbonate assemblage may occur in sharp contact to the assemblage type I.

**Type III**. A carbonate-rich magnetite-chlorite/amphibole-quartz assemblage contains up to 25 vol. % of carbonates (Fig. 5, layers C and F), which are typically concentrated in form of lensoidal aggregates. In some parts quartz is nearly absent (Fig. 6, layer B) whereas other layers are quartz-rich (Fig. 6, layer A). Quartz-rich layers are relatively magnetite-rich (Fig. 5, layer C), whereas domains with lower quartz contents are enriched in mixture of magnetite and chlorite/amphibole (Fig. 6, layer B). This type is a transition between the two above-mentioned assemblages.

**Type IV**. All the three above-mentioned assemblages form the ore body which is associated with a carbonate-free ore-bearing rock consisting of predominant chlorite, and subordinate amphibole. The rock is fine-grained, compact and dark-green in colour. Other rock constituents are magnetite and quartz which together do not exceed 20 vol. %. Based on its mineralogy, the rock can be classified as a chlorite-amphibole schist. In the text, tables and diagrams this rock is distinguished as the rock type IV.

## 6. Results

### 6.1. Petrography

Due to its high Fe-content, in transmitted light, chlorite is of green colour and therefore similar to amphibole. Additionally, chlorite occurs always in close association with amphibole which it replaces. These are the reasons that the two minerals are hardly distinguishable from each other. Generally, chlorite is often distinctly more abundant than amphibole. Amphibole forms tiny and elongated crystals (30 to 50 μm in length and about 3 μm thick) that occur in the form of felty aggregates (Fig. 7a). These general features were observed in three mineral assemblages I–III and in the crenulation-cleavage textured rock type IV:

- Carbonate-bearing magnetite-chlorite/amphibole-quartz assemblage-(I). This assemblage forms weakly developed layers of different mineral composition. The most abundant layer type is rich in magnetite (30 to 50 vol. %) which occurs in a groundmass consisting of chlorite and/or amphibole. Magnetite forms euhedral to subhedral crystals (grain sizes between 0.015 to 0.4 mm; on average 0.15 mm) clustered mainly to polycrystalline aggregates. These are intimately intergrown with amphibole aggregates which are mainly replaced by chlorite. In proportions by far smaller than 1 vol. %, biotite occurs in association with chlorite and/or amphibole. Biotite may be coarse-grained (grain size up to 2 mm) and is partially replaced by chlorite (Fig. 7b). Quartz is inhomogeneously distributed and its amount varies between 10 and 30 vol. %. It is mainly concentrated in polycrystalline masses arranged parallel to the metamorphic schistosity. Its amount increases obviously on the expense of amphibole and/or chlorite. The grain boundaries between amphibole and/or chlorite and quartz are irregular and quartz may contain small relics of amphibole and chlorite (Fig. 7c). Of minor abundance are tiny ilmenite crystals and euhedral to subhedral quartz grains in those layers that consist of magnetite and chlorite/amphibole. Carbonates are rare and they are irregularly distributed. Apart from magnetite, pyrrhotite may also occur in some samples of this assemblage. However, if pyrrhotite occurs, it is locally abundant and often closely associated with magnetite (Fig. 7d). The inclusions form small droplet-shaped bodies (0.003 to 0.01 mm) or aggregates (up to 0.09 mm) in which the crystals are arranged in granoblastic triple-junction configuration (Fig. 8). Pyrrhotite may contain small inclusions of chalcopyrite and may be altered into pyrite in the morphological form of “bird eyes” due to supergene weathering (Fig. 8).

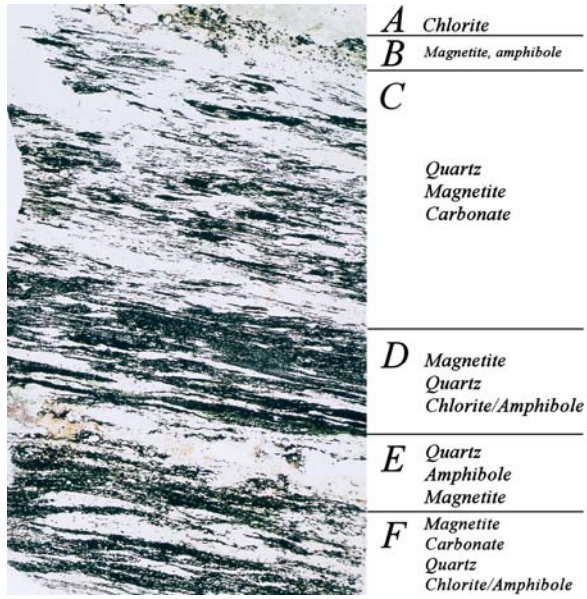


Fig. 5. Carbonate-rich magnetite-amphibole/chlorite-quartz assemblage type III (sample 861/12) containing layered arranged magnetite (black) that is associated with chlorite, carbonate, quartz and amphibole (sublayers A to F). Carbonate is concentrated in sublayers C and F often in the form of lensoidal shaped bodies (especially in F). Transmitted light, 4.5×2.5 cm.

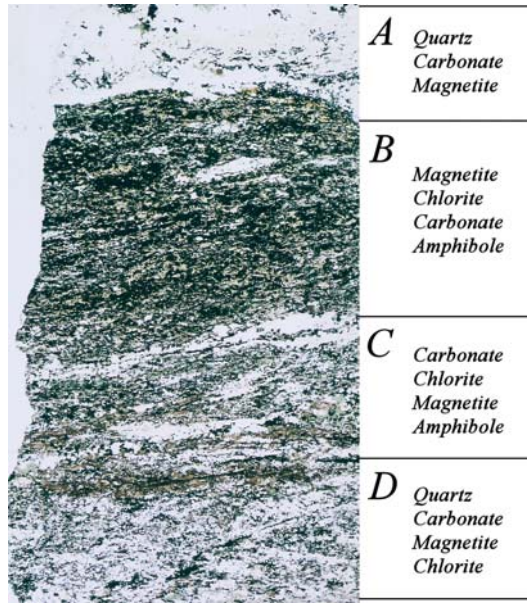


Fig. 6. Carbonate-rich magnetite-chlorite/amphibole-quartz assemblage type III (sample 861/9) consisting of sublayers (A to D) showing different proportions of carbonate (increasing from C via D to A). Sublayer B consisting predominantly of magnetite and chlorite/amphibole, contains small amounts of carbonate in the form of lensoidal shaped bodies. Transmitted light, 4.5×2.5 cm.

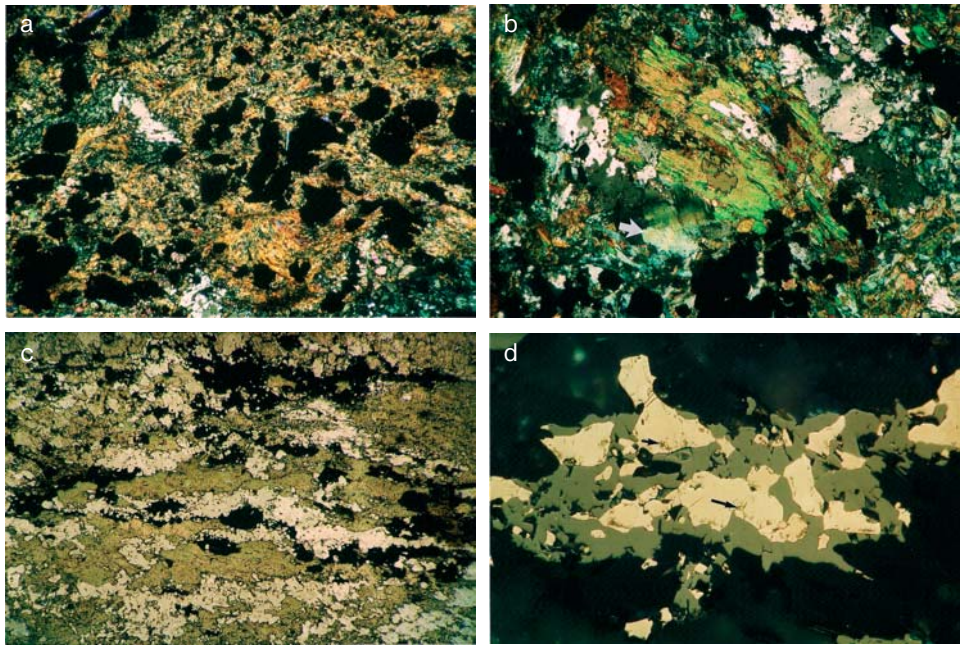


Fig. 7. Optical microscope photographs of mineral textures.
a: Euhedral to subhedral magnetite crystals or aggregates of them (black) in amphibole (consisting of finely-felted aggregates) and subordinate quartz (white to grey). Transmitted light, crossed polars, length of the longer edge 10.5 mm.
b: Coarse-grained biotite crystal (in the centre) associated with quartz, amphibole, magnetite (black) and chlorite (arrow). Transmitted light, length of the longer edge 10.5 mm.
c: Chlorite (greenish), magnetite (black) and quartz (white) showing irregular grain boundaries of chlorite and magnetite in contact to quartz. Transmitted light, length of the longer edge 10.5 mm.
d: Coarse-grained pyrrhotite crystals (slightly altered; small arrows) in magnetite embedded in chlorite/amphibole (dark). Reflected light, oil immersion, longer edge 450 μm.

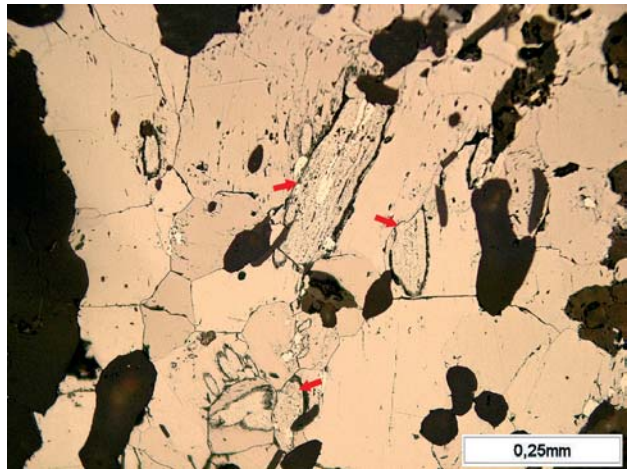


Fig. 8. Pyrrhotite (anisotropic) in metamorphic triple-junction configuration. Note the beginning alteration into pyrite (arrows). Reflected light, oil immersion, longer edge 450 μm.

- Carbonate-dominated magnetite-chlorite/amphibole-quartz assemblage-(II). The layer-like arranged carbonate is the dominating mineral of this assemblage (up to 80 vol. %). It contains aggregates of magnetite (up to 20 vol. %) that occur in the form of elongated, lenticular bodies. These bodies are parallel to each other (Fig. 9a). Other constituents are small amounts of chlorite and/or amphibole (up to 5 vol. %) and sporadically biotite and apatite. Quartz varies from about 5 to 20 vol. % and its amount increases at the expense of carbonate.

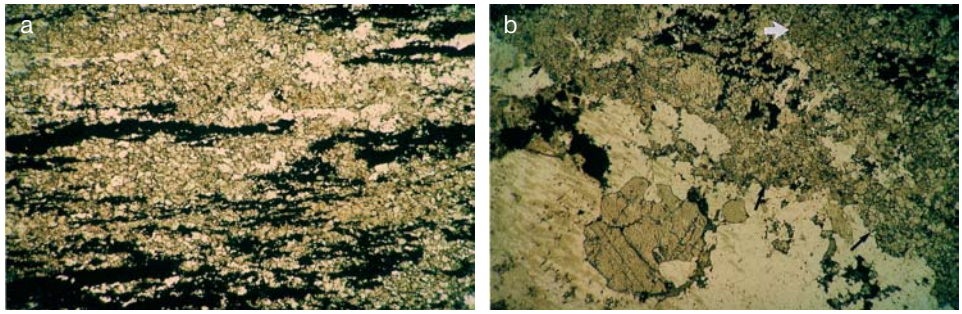


Fig. 9. Optical microscope photographs of the ore.
a: Layered distribution of magnetite (black), carbonate and quartz (white). Transmitted light, length of the longer edge 10.5 mm.
b: Carbonate (long arrows), chlorite/amphibole (short and white arrows) and quartz containing a big apatite crystal (2.4 mm). Note the corroded contacts of the minerals to quartz. Transmitted light, length of the longer edge 10.5 mm.

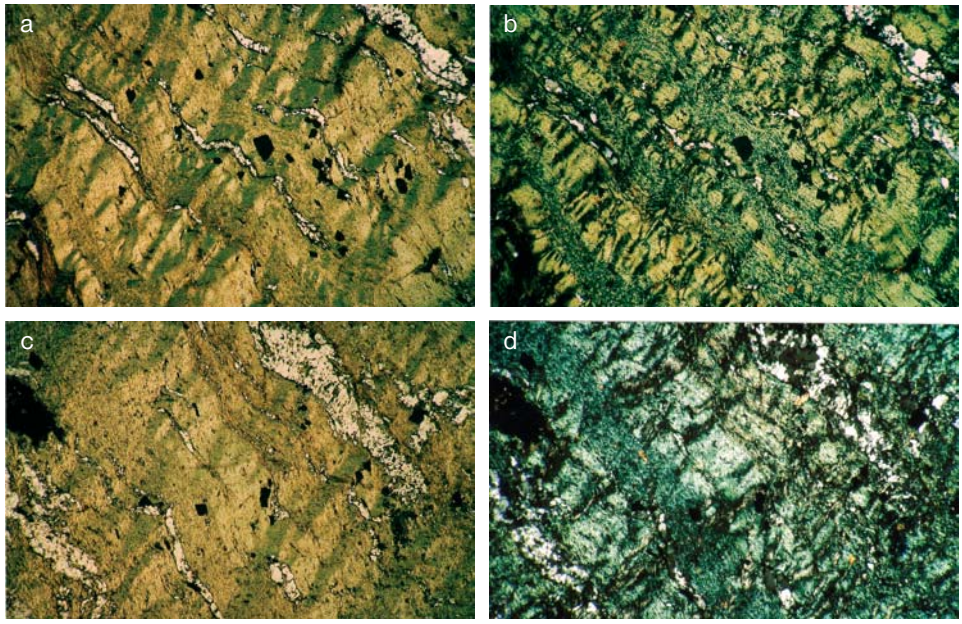


Fig. 10. Optical microscope photographs of ore textures.
a: Crenulation-cleavage textured amphibole containing magnetite crystals (black) and quartz (white) following the planes of the crenulation cleavage. Transmitted light, length of the longer edge 10.5 mm;
b: Identical with Fig. 10a, but with crossed polars.
c: Chlorite replacing pseudomorphically the crenulation-cleavage textured amphibole associated with magnetite (black) and quartz (white). Transmitted light, length of the longer edge 10.5 mm.
d: Identical with Fig. 10c, but with crossed polars.

- Carbonate-rich magnetite-chlorite/amphibole-quartz assemblage-(III). The above-described two types are often connected by transitions formed by assemblages in which carbonate and magnetite-chlorite/amphibole layers occur in alternating setting. It was also observed, that magnetite-dominated layers contain not only chlorite and/or amphibole, but also carbonate either in the form of single grains or as lensoidal polycrystalline bodies. Quartz occurs in quantities up to 30 vol. % and may contain ilmenite and apatite of which one crystal was found having a diameter of about 2 mm (Fig. 9b).
- Rock type IV (chlorite-amphibole schist). This rock type differs from the other three assemblages by the absence of carbonate, the occurrence of an older amphibole-generation, the development of the crenulation-cleavage texture and the absence of Sr in the whole-rock composition. More than 75 vol. % of this rock consists of chlorite and subordinately of amphibole. The elongated amphibole crystals (generation-II), containing irregularly shaped relics of an older amphibole (generation-I), are fine-grained and occur in the form of very small, parallel lying needle-like crystals which are arranged in the crenulation-cleavage texture (Fig. 10 a, b). Identical arrangement exhibit also chlorite crystals. This is due to the fact that amphibole-II is pseudomorphosed by chlorite (Fig. 10c, d). Relics of amphibole-I may also occur in newly-formed chlorite (Fig. 11a). The replacement of amphibole by chlorite is inhomogeneously distributed, with the result that domains within the rock consist of amphibole or chlorite only or of mixtures of both. However, chlorite is by far the predominating mineral. Ilmenite is relatively abundant (locally up to 5 vol. %) forming elongated euhedral crystals (length 15 to 40 μm). These crystals follow the patterns of amphibole/chlorite (Fig. 11b). Magnetite (up to 10 vol. %) occurs in the form of locally enriched euhedral to subhedral crystals (0.02 to 0.4 mm, on average 0.1 mm) and may contain very small droplet-like inclusions of pyrrhotite. Similar to the arrangement of ilmenite is that of graphite (about 1 vol. %) which forms elongated, wave-like deformed crystals. Quartz is inhomogeneously distributed (up to 10 vol. %) and its occurrence reflects the rock texture (Figs. 10a, c).

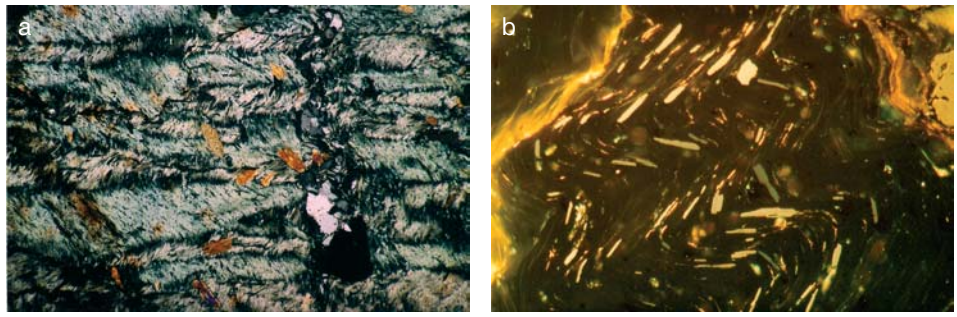


Fig. 11. Optical microscope photographs of the rock type IV.
a: Irregular distributed relics of amphibole-I (= ferrotschermakite) in chlorite arranged in the crenulation-cleavage texture. Other minerals are quartz and magnetite (black). Transmitted light, crossed polars, length of the longer edge 3.5 mm.
b: Elongated ilmenite crystals following the crenulation-cleavage texture of amphibole in which it is embedded. Reflected light, oil immersion, not exactly crossed polars, longer edge 450 μm.

### 6.2. Whole-rock analyses

The whole-rock compositions are summarized in Tab. 1 containing the analytical data of the three assemblage types (I–III) and of rock type IV. Apart from the oxides $SiO_2$, $Al_2O_3$, $Fe_2O_3$, CaO and the LOI-content, the other oxides do not show significant differen-

ces. $SiO_2$ has the highest values in assemblage type I (36.30 to 46.47 wt. %). Lower $SiO_2$-contents occur in the types III and IV ranging from 26.09 to 28.22 wt. %. Whereas $SiO_2$ of the type II is widely identical with the amount of quartz, the $SiO_2$-content of the type IV is mainly related to the contents of chlorite and amphibole. In the other two types, $SiO_2$ occurs either in the form of quartz or is constituent of chlorite and amphibole. The $Al_2O_3$-content of the assemblages I, II and III lies in a small range between 1.51 and 4.19 vol. % and is mainly bound to the chlorite (containing on average about 20 wt. % $Al_2O_3$). An exception is the high $Al_2O_3$-concentration (about 14 wt. %) of type IV that consists predominantly of chlorite and subordinate amphibole.

Table 1. Whole-rock analyses in wt. % (upper part) including trace-element concentrations in ppm (lower part) of the assemblages I–III, rock type IV and chlorite schist of Fojt *et al.* (1993). The last line contains the amount of Fe expressed as $FeO_{tot}$ (wt. %). nd = not detected; na = not analysed.

| | **Assemblage I** | | | | | **Assemblage II** | | **Assemblage III** | | **Rock type IV** | |
|---|---|---|---|---|---|---|---|---|---|---|---|
| Sample | 861/1 | 861/1 | 861/3 | 861/7 | 861/2 | 861/4 | 861/6 | 861/9 | 861/12 | 861/10 | Fojt |
| $SiO_2$ | 41.04 | 41.00 | 46.47 | 38.89 | 36.30 | 26.09 | 28.08 | 30.00 | 31.67 | 28.22 | 26.10 |
| $TiO_2$ | 0.10 | 0.08 | 0.06 | 0.34 | 0.22 | 0.08 | 0.18 | 0.31 | 0.12 | 0.47 | 2.44 |
| $Al_2O_3$ | 2.99 | 2.24 | 1.51 | 2.56 | 4.19 | 2.73 | 4.11 | 3.36 | 2.02 | 14.54 | 13.78 |
| $Fe_2O_3$ | 21.15 | 25.10 | 26.35 | 26.38 | 26.93 | 5.33 | 6.88 | 11.77 | 16.22 | 13.55 | 14.91 |
| FeO | 27.40 | 24.60 | 21.44 | 21.35 | 23.72 | 22.30 | 22.79 | 23.03 | 25.75 | 29.29 | 29.22 |
| MnO | 0.18 | 0.16 | 0.05 | 0.04 | 0.07 | 0.19 | 0.24 | 0.21 | 0.14 | 0.03 | 0.05 |
| MgO | 1.57 | 1.56 | 0.49 | 0.57 | 1.18 | 1.94 | 2.68 | 1.75 | 1.43 | 3.00 | 1.02 |
| CaO | 1.32 | 1.18 | 0.69 | 3.91 | 4.16 | 17.10 | 14.40 | 11.81 | 9.39 | 1.87 | 3.34 |
| $Na_2O$ | 0.42 | <0.10 | n.d. | 0.36 | n.d. | n.d. | n.d. | 0.16 | n.d. | n.d. | 0.10 |
| $K_2O$ | 0.33 | 0.22 | 0.04 | 0.15 | 0.06 | 0.01 | 0.03 | 0.37 | 0.04 | 0.02 | 0.09 |
| $P_2O_5$ | 0.20 | 0.12 | 0.12 | 0.38 | 0.15 | 0.07 | 0.09 | 0.19 | 0.17 | 0.09 | 0.80 |
| $SO_3$ | 2.32 | n.a. | 1.69 | 0.05 | 0.07 | 0.59 | 0.78 | 2.72 | 1.62 | 0.01 | n.a. |
| LOI | 0.71 | 0.75 | 0.49 | 2.21 | 2.16 | 22.19 | 18.48 | 13.48 | 11.07 | 7.38 | 7.00 |
| $H_2O^-$ | 0.16 | 0.17 | 0.10 | 0.08 | 0.16 | 0.28 | 0.38 | 0.21 | 0.25 | 0.63 | 0.20 |
| | **99.98** | **97.18** | **99.50** | **99.27** | **99.37** | **98.90** | **99.45** | **99.37** | **99.89** | **99.10** | **100.01** |
| V | 41 | 42 | 81 | 62 | 109 | 35 | 54 | 66 | 66 | 115 | 200 |
| Cr | 15 | <5 | <5 | 22 | 30 | 10 | 8 | 35 | 8 | 67 | 200 |
| Co | 56 | 14 | 45 | 34 | 51 | 16 | 8 | 21 | 27 | n.d. | n.a. |
| Ni | 19 | 48 | n.d. | 30 | 23 | 9 | 17 | 34 | 13 | 48 | 47 |
| Cu | n.d. | n.a. | n.d. | n.d. | n.d. | n.d. | 14 | 46 | 48 | n.d. | 21 |
| Zn | 46 | 40 | 38 | 41 | 53 | 40 | 55 | 42 | 37 | 129 | 103 |
| Rb | 38 | 36 | n.d. | 11 | n.d. | n.d. | 2 | 44 | 1 | 4 | n.a. |
| Sr | 87 | 144 | 14 | 94 | 89 | 298 | 226 | 202 | 161 | <3 | n.a. |
| Zr | 13 | 38 | 11 | 22 | 27 | 13 | 32 | 34 | 17 | 87 | n.a. |
| Ba | 54 | 56 | 9 | 67 | 36 | 21 | 15 | 125 | 6 | 16 | 166 |
| $Fe_{tot}$ | 46.43 | 47.18 | 45.15 | 45.09 | 47.95 | 27.10 | 28.98 | 33.62 | 40.34 | 41.48 | 42.64 |

### 6.3. REE analyses

Tab. 2 contains the REE-analyses (in ppm) of the assemblage type I–III and rock type IV. The analytical data show that the contents of ΣREE in all assemblages are low. Type IV has the lowest ΣREE-content (21.65 ppm). In the other rocks ΣREE varies between 35.67 and 64.55 ppm. Values lying close to 64 ppm were found in those samples that contain the highest $Na_2O$ and $K_2O$ concentrations of the whole-rock composition. In the other samples with distinctly lower ΣREE values (35.67–53.87 ppm) amphibole is mainly replaced by chlorite. This interpretation would also explain the low ΣREE content of rock type IV in which amphibole is nearly completely replaced by chlorite.

Table 2. ICP-MS analyses of the REE (in ppm) of assemblages type I–III and rock type IV.

| | Assemblage I | | | | Assemblage II | | Assemblage III | | IV |
|---|---|---|---|---|---|---|---|---|---|
| Sample | 861/1 | 861/2 | 861/3 | 861/7 | 861/4 | 861/6 | 861/9 | 861/12 | 861/10 |
| La | 13.68 | 9.37 | 8.22 | 14.63 | 10.92 | 8.28 | 13.83 | 8.70 | 3.54 |
| Ce | 22.00 | 12.08 | 13.30 | 21.81 | 17.55 | 13.84 | 20.95 | 14.83 | 6.96 |
| Pr | 3.42 | 1.89 | 1.95 | 3.45 | 2.60 | 1.99 | 3.19 | 2.19 | 1.15 |
| Nd | 13.69 | 7.87 | 7.41 | 13.84 | 10.58 | 7.97 | 12.97 | 8.89 | 4.90 |
| Sm | 2.78 | 1.63 | 1.42 | 2.74 | 2.40 | 1.81 | 2.99 | 1.98 | 1.18 |
| Eu | 0.60 | 0.34 | 0.27 | 0.67 | 0.83 | 0.48 | 0.82 | 0.35 | 0.25 |
| Gd | 2.57 | 1.70 | 1.17 | 2.47 | 2.58 | 2.04 | 3.04 | 2.12 | 1.07 |
| Tb | 0.35 | 0.25 | 0.15 | 0.33 | 0.42 | 0.34 | 0.46 | 0.34 | 0.16 |
| Dy | 1.99 | 1.43 | 0.72 | 1.74 | 2.45 | 2.07 | 2.64 | 2.00 | 0.93 |
| Ho | 0.39 | 0.29 | 0.14 | 0.32 | 0.48 | 0.44 | 0.50 | 0.40 | 0.18 |
| Er | 1.13 | 0.87 | 0.37 | 0.84 | 1.35 | 1.31 | 1.42 | 1.16 | 0.54 |
| Tm | 0.16 | 0.13 | 0.06 | 0.12 | 0.19 | 0.12 | 0.20 | 0.16 | 0.08 |
| Yb | 1.09 | 0.91 | 0.42 | 0.77 | 1.33 | 1.46 | 1.34 | 1.21 | 0.61 |
| Lu | 0.16 | 0.14 | 0.07 | 0.12 | 0.19 | 0.24 | 0.20 | 0.19 | 0.10 |
| ΣREE | 64.01 | 38.90 | 35.67 | 63.85 | 53.87 | 43.39 | 64.55 | 44.62 | 21.65 |
| ΣLREE | 56.17 | 33.18 | 32.57 | 57.14 | 44.88 | 34.37 | 54.75 | 37.04 | 17.98 |
| ΣHREE | 7.84 | 5.72 | 3.10 | 6.71 | 8.99 | 8.02 | 9.80 | 7.58 | 3.67 |
| ΣL/ ΣH | 7.16 | 5.58 | 10.51 | 8.52 | 4.99 | 4.29 | 5.59 | 4.87 | 4.90 |
| Eu/Sm | 0.22 | 0.21 | 0.19 | 0.24 | 0.35 | 0.27 | 0.27 | 0.18 | 0.21 |

### 6.4. Fluid inclusions

Fluid inclusions were identified within both quartz and carbonate. Quartz contains five types of fluid inclusions. Type Q1 ($CO_2$-$H_2O$) FI are present in all samples investigated, but in relatively small quantity. FI are typically small (up to 11 μm), present as solitary or in small three-dimensional clusters which is indicative for early ("primary") timing (TOURET 2001). Shapes are isometric. At room temperatures the following phases are visible: liquid $CO_2$-rich phase ($L_{car}$), aqueous solution ($L_{aq}$), sometimes also vapour phase ($V_{car}$), and/or an accidentally trapped birefringend solid phase. The phase proportions of carbonic and aqueous phases vary broadly from approximately 40 to 70 vol. % of carbonic phase. Homogenization of $CO_2$ phase occurred between –2.4 and +27.9 °C, and the mode of homogenization was to liquid in all cases. During heating many inclusions decrepitated even before total homogenization. Only few FI were successfully homogenized by either 1) dissolution of minor $CO_2$ phase in aqueous solution or 2) dissolution of minor aqueous solution in carbonic phase. In the first case, the Th-tot values vary broadly from 435 to >550 °C (Tab. 3). In the second case, the accurate Th-tot value typically cannot be precisely measured due to optical reasons: it can be concluded only, that the Th-tot is higher then ca. 300 °C. One inclusion with a small tip showed Th-tot as high as 432 °C. Solid phases do not dissolve during heating. The solid $CO_2$ phase melted at temperatures between –57.3 and –59.3 °C with most measurement down to –57.6 °C. The melting of ice was observed in a water-dominated inclusion at –3.3 °C. The melting of clathrate was observed between +7.9 °C and +9.7 °C with the highest measured value being found in $CO_2$-rich inclusion (sample MD). The Type Q1 FI contains 55–84 mol. % $H_2O$, 15–45 mol. % $CO_2$ and 0.1–1.1 mol. % NaCl, if their composition is approximated by the system $CO_2$-$H_2O$-NaCl. In addition, small amount of non-condensable gas (possibly ca 5–10 mol. % of methane or nitrogen in the vapour mixture, THIÉRY *et al.* 1994) is

indicated by lowering of melting temperature of solid $CO_2$ down to the theoretical value of –56.6 °C.

Type Q2 ($CO_2$) FI are relatively more frequent when compared to the Q1 type. They are typically present in short trails not cutting the whole quartz grain, which possibly represent ancient healed microfractures. At room temperature, they appear to be one-phase ($L_{car}$) or two-phase ($L_{car} + V_{car}$). The microthermometric parameters are similar to those characterizing the $CO_2$ phase of Type Q1 inclusions (Tab. 3). These FI may possibly contain a small amount (up to 10 vol. %) of aqueous solution which is optically invisible (e.g., VAN DEN KERKHOF and THIÉRY 1994). In such a case, the fluid would be formed by min. 75 mol. % $CO_2$, up to 25 mol. % $H_2O$ and up to 0.1 mol. % NaCl.

Type Q3 ($H_2O$-$CO_2$) FI are flat, evidently arranged along healed microfractures. FI typically contain dominating aqueous solution (c. 95 vol. %) and minor $CO_2$ phase (around 5 vol. %). Occasionally the birefringend solid phase was observed which dissolved at 149 °C (one observation). The Th-tot range between 207 and 261 °C. Cryometric parameters mostly cannot be measured due to small sizes of the present FI.

Type Q4 ($H_2O$) FI are evidently secondary. They are flat with irregular shape and up to 27 μm in size. FI are exclusively two-phase (L + V) at room temperature, with consistent liquid-vapour ratios (the vapour phase takes approx. 5 vol. %). The microthermometric parameters differ in both samples where these FI have been observed (Tab. 3). The homogenization temperatures are generally low (129–189 °C) and the salinities are variable (between 15.8 and 17.0 wt. % NaCl equiv. for sample MD, 0.0 wt. % NaCl equiv. for sample MD2).

Type Q5 ($CH_4$) FI occur along healed microfractures and are frequently present in all quartz samples. They are very dark, flat or three-dimensional with both irregular shape and often tiny tips and up to 22 μm in size. They seem to be monophase at room temperature. On cooling, a liquid phase condenses below –100 °C. Further cooling down to temperature limit of the apparatus (–196 °C) does not initiate other phase changes. On reheating, the inclusions homogenize to vapour at temperatures between –97.5 and –100.1 °C (Tab. 3). The inclusions probably contain low-density methane-dominating fluid.

Carbonate exhibits relatively easier situation than quartz from fluid inclusion point of view. Only two types of fluid inclusions have been recognized. C1 primary inclusions belonging to type $CO_2$ are abundant in ankerite, but are typically very small (up to 10 μm) and concentrated around the centre of the carbonate grain whereas the rim is essentially inclusion-free. They exhibit a negative-crystal shape or are quiet irregular. The FI are monophase ($L_{car}$) or two phase ($L_{car} + V_{car}$) at room temperature. The fluid inclusions exhibit similar parameters to those characterizing the $CO_2$-dominating Q2-type FI in quartz (Tab. 3).

C2 FI of problematic origin belonging to type $H_2O$ are present in both calcite and ankerite. FI typically occur as solitary with no relation to fractures, but exhibit very flat and irregular morphology indicative for secondary FI. Phase composition varies across the samples: L-only FI was found in sample MD whereas L+V FI are present in sample MD3. The calcite hosted inclusion showed $Tm_{ice}$ as high as –2.0 °C indicating salinity of 3.4 wt. % NaCl equiv. In sample MD3 the homogenization temperatures are very low (72 and 75 °C). The cryometric parameters cannot be measured here due to small sizes of the present FI.

Table 3. Results of microthermometric measurements of fluid inclusions from Malý Děd. Temperature parameters are in °C. All Th $CO_2$-phase values are to the liquid state and all Th $CH_4$-phase values are to the vapour, respectively. LVR – liquid-vapour ratio, d – decrepitation temperature.

**1) $CO_2$-bearing FI**

| Sample | Mineral | FI type | Vol. % $CO_2$ | Th-tot | Th $CO_2$-phase | Tm $CO_2$ | Tm cla |
|---|---|---|---|---|---|---|---|
| MD | Quartz | Q1 | ~ 30–40 | 435–>550 | +10.1/+26.3 | –57.4/–59.3 | +7.9 |
| | | | ~ 70 | | +14.0/+27.9 | –57.6/–59.2 | +9.7 |
| MD1 | Quartz | Q1 | ~ 40 | 227–289 (d) | –2.4/+18.3 | –57.3 | +8.5/+9.4 |
| | | | ~ 60 | 432 | –2.6/+26.2 | –57.3 | |
| | | Q2 | 100 ? | | –0.4 | –57.5 | |
| | | Q3 | 5–10 | 207–261 | | | +8.7 |
| MD2 | Quartz | Q1 | ~ 60 | 211–265 (d) | +20.5/+22.0 | –57.3 | +8.4/+8.9 |
| | | Q2 | 100 ? | | +20.5/+28.2 | –57.3/–57.5 | |
| | Ankerite | C1 | 100 ? | | +20.1/+25.8 | –57.6 | |

**2) Aqueous FI**

| Sample | Mineral | FI type | Phase composition | LVR | Th (L+V) | Te | Tm ice |
|---|---|---|---|---|---|---|---|
| MD | Quartz | Q4 | L+V | 0.95 | 145–189 | –53 | –11.8/–13.1 |
| | Calcite | C2 | L | 1.00 | | | –2.0 |
| MD2 | Quartz | Q4 | L+V | 0.95 | 129 | | 0.0 |
| MD3 | Ankerite | C2 | L+V | 0.95 | 72–75 | | |

**3) $CH_4$-bearing FI**

| Sample | Mineral | FI type | Th $CH_4$-phase |
|---|---|---|---|
| MD | Quartz | Q5 | –97.5/–97.6 |
| MD1 | Quartz | Q5 | –98.1/–98.5 |
| MD2 | Quartz | Q5 | –99.2/–100.1 |

## 6.5. Mineral chemistry

*Amphibole* at the locality is represented by two distinct types: calcic amphibole-(I) restricted to the rock type IV and iron-magnesian amphibole-(II) which was found in the whole ore body (assemblages I to III) and in rock type IV. Despite of its widespread distribution, the amphibole-(II) compositions are relatively constant (Table 4). Calcic amphibole-(I) exhibits relatively high CaO (9.99 to 10.64 wt. %), $Na_2O$ (0.89 to 1.10 wt. %) and $K_2O$ (0.25 to 0.30 wt. %). The other oxides vary between 25.90 and 26.74 wt. % for FeO, 0.62 and 2.22 wt. % for MgO and 17.59 and 21.33 wt. % for $Al_2O_3$. On the other hand, amphibole-(II) has only low contents of CaO (0.14 to 1.96 wt. %), $Na_2O$ (0.03 to 0.19 wt. %) and $K_2O$ (0.00 to 0.04 wt.%) and its content of major oxides vary between 37.74 and 42.39 wt. % for FeO, 5.31 and 7.49 wt. % for MgO and 0.27 and 3.64 wt. % for $Al_2O_3$.

*Biotite* is a rare mineral and occurs in association with amphibole and/or chlorite (assemblages I and III). Its amount does not exceed 1 vol. %. In some cases the porphyroblastic grains are relatively big (Fig. 7b). Biotite has high content of FeO (about 30 wt. %) and low of MgO (4.0 to 5.7 wt. %) (Tab. 5).

*Chlorite* is the most widespread mineral of Malý Děd and occurs in all samples. It is most abundant in rock type IV. More than 40 analyses of chlorite were carried out showing that this mineral is relatively constant in composition. Eight analyses are presented in Table 5. The highest variations exhibit FeO (37.86 to 43.67 wt. %) and MgO (2.19 to 5.99 wt. %).

Table 4. Representative analyses of amphibole-(I) and amphibole-(II) in wt. % (upper part) and apfu (lower part) showing minimal and maximal oxide contents.

| | **Calcic amphibole (amphibole-I)** | | | | **Fe-Mg amphibole (amphibole-II)** | | | | | |
|---|---|---|---|---|---|---|---|---|---|---|
| $SiO_2$ | 37.35 | 38.95 | 37.36 | 40.37 | 49.86 | 48.03 | 49.46 | 50.56 | 49.93 | 50.20 |
| $TiO_2$ | 0.08 | 0.14 | 0.14 | n.d. | n.d. | n.d. | n.d. | n.d. | n.d. | n.d. |
| $Al_2O_3$ | 21.33 | 19.90 | 20.88 | 17.59 | 0.72 | 3.64 | 1.57 | 0.27 | 0.92 | 0.34 |
| $FeO_{anal.}$ | 26.74 | 25.90 | 26.43 | 26.27 | 42.39 | 37.74 | 38.66 | 40.36 | 39.77 | 39.54 |
| MnO | 0.03 | 0.04 | 0.03 | 0.31 | 0.25 | 0.62 | 0.74 | 0.71 | 0.51 | 0.25 |
| MgO | 0.62 | 0.98 | 1.13 | 2.22 | 5.47 | 5.31 | 6.10 | 6.38 | 7.07 | 7.49 |
| CaO | 10.42 | 10.47 | 10.64 | 9.99 | 0.19 | 1.96 | 1.18 | 0.14 | 0.30 | 0.25 |
| $Na_2O$ | 0.82 | 0.77 | 0.89 | 1.10 | 0.08 | 0.19 | 0.06 | 0.03 | 0.09 | 0.04 |
| $K_2O$ | 0.28 | 0.30 | 0.30 | 0.25 | n.d. | 0.04 | 0.04 | n.d. | n.d. | n.d. |
| $FeO_{calc.}$ | 21.22 | 22.49 | 19.94 | 21.93 | 42.00 | 37.74 | 38.66 | 40.36 | 38.79 | 38.59 |
| $Fe_2O_{3calc.}$ | 6.14 | 3.79 | 7.21 | 4.82 | 0.43 | – | – | – | 1.09 | 1.06 |
| $H_2O_{calc.}$ | 1.96 | 1.95 | 1.96 | 1.97 | 1.89 | 1.89 | 1.89 | 1.90 | 1.91 | 1.90 |
| Total | **100.25** | **99.78** | **100.48** | **100.55** | **100.89** | **99.42** | **99.70** | **100.35** | **100.61** | **100.12** |
| Si | 5.717 | 5.973 | 5.699 | 6.144 | 7.895 | 7.630 | 7.841 | 7.992 | 7.837 | 7.900 |
| Al | 2.283 | 2.027 | 2.301 | 1.856 | 0.105 | 0.370 | 0.159 | 0.008 | 0.163 | 0.063 |
| Σ | **8.000** | **8.000** | **8.000** | **8.000** | **8.000** | **8.000** | **8.000** | **8.000** | **8.000** | **7.963** |
| Al | 1.565 | 1.569 | 1.453 | 1.299 | 0.029 | 0.312 | 0.134 | 0.042 | 0.007 | – |
| Ti | 0.009 | 0.017 | 0.016 | – | – | – | – | – | – | – |
| $Fe^{3+}$ | 0.707 | 0.437 | 0.828 | 0.552 | 0.051 | – | – | – | 0.129 | 0.125 |
| Mg | 0.142 | 0.224 | 0.257 | 0.504 | 1.291 | 1.257 | 1.441 | 1.504 | 1.654 | 1.757 |
| $Fe^{2+}$ | 2.577 | 2.753 | 2.446 | 2.645 | 5.564 | 5.014 | 5.126 | 5.335 | 5.092 | 5.079 |
| Mn | – | – | – | – | 0.033 | 0.083 | 0.099 | 0.095 | 0.068 | 0.033 |
| Ca | – | – | – | – | 0.032 | 0.334 | 0.200 | 0.024 | 0.050 | 0.043 |
| Σ | **5.000** | **5.000** | **5.000** | **5.000** | **7.000** | **7.000** | **7.000** | **7.000** | **7.000** | **7.037** |
| $Fe^{2+}$ | 0.139 | 0.132 | 0.098 | 0.147 | – | – | – | – | – | – |
| Mn | 0.004 | 0.006 | 0.004 | 0.040 | – | – | – | – | – | – |
| Ca | 1.709 | 1.720 | 1.739 | 1.629 | – | – | – | – | – | – |
| Na | 0.148 | 0.142 | 0.159 | 0.184 | 0.025 | 0.058 | 0.018 | 0.009 | 0.027 | 0.012 |
| K | – | – | – | – | – | 0.008 | 0.008 | – | – | |
| Σ | **2.000** | **2.000** | **2.000** | **2.000** | **0.025** | **0.066** | **0.026** | **0.009** | **0.027** | **0.012** |
| Na | 0.096 | 0.087 | 0.104 | 0.141 | – | – | – | – | – | – |
| K | 0.054 | 0.059 | 0.059 | 0.048 | – | – | – | – | – | – |
| Σ | **0.150** | **0.146** | **0.163** | **0.189** | – | – | – | – | – | – |
| OH | 2.000 | 2.000 | 2.000 | 2.000 | 2.000 | 1.992 | 1.999 | 1.957 | 2.000 | 2.000 |
| O | – | – | – | – | – | 0.008 | 0.001 | 0.043 | – | – |
| Σ | **2.000** | **2.000** | **2.000** | **2.000** | **2.000** | **2.000** | **2.000** | **2.000** | **2.000** | **2.000** |
| ΣO | **22.000** | **22.000** | **22.000** | **22.000** | **22.000** | **22.000** | **22.000** | **22.000** | **22.000** | **22.000** |
| Mg-# | **0.05** | **0.07** | **0.13** | **0.15** | **0.19** | **0.20** | **0.22** | **0.22** | **0.25** | **0.26** |

The chemical composition of *carbonates* is summarized in the Tabs. 6 to 9. The data show that the carbonates are composed of ankerite-dolomite solid solutions and calcite. Whereas calcite is restricted to mineral assemblage I, ankerite-dolomite occurs in all the assemblages, but is of minor abundance in assemblage I.

*Ankerite-dolomite* is always zoned (Figs. 12a, b and d). The core of the crystals contains the highest content of $CaFe(CO_3)_2$ (75.14 to 85.70 mol. %) and the lowest of $CaMg(CO_3)_2$ (23.46 to 10.94 mol. %). Along the rim, the dolomite component ranges from 40.10 to 25.72 mol. % and the ankerite component from 56.60 to 75.14 mol. %. Other constituents of ankerite-dolomite are $CaMn(CO_3)_2$ and $CaSr(CO_3)_2$ (up to 2.06 and

0.48 mol. %, respectively). The analyses of ankerite-dolomite show always excess of $CaCO_3$ in the range between 0.10 and 5.14 mol. %. Generally, this Ca excess can be as large as 8 mol. % and occurs as $CaCa(CO_3)_2$ in the ankerite solid solution (REEDER and DOLLASE, 1989). In the assemblages II and III, calcite (Fig. 12a) or siderite (Fig. 12d) or siderite + calcite (Fig. 12b) form inclusions in the ankerite-dolomite. Calcite contains up to 24.19 mol. % $FeCO_3$ and 6.16 mol. % $MgCO_3$ and siderite up to 13.11 mol. % $CaCO_3$.

*Calcite*, the dominating carbonate mineral of assemblage I is mainly distributed in the form of sporadically occurring single crystals (Fig. 13a) or in irregular to lenticular polycrystalline aggregates (Fig. 3, layers A and D). Calcite contains 5.31 to 10.46 mol. % $FeCO_3$, low quantities of $MnCO_3$ and rare also $MgCO_3$ in the solid solution. Calcite has always small and irregularly shaped inclusions of siderite (Figs. 13a, b) and rarely ankerite (Fig. 13b).

Table 5. Selected chlorite and biotite analyses in wt. % (upper part) and apfu (medium part). The lower part contains the concentration of $Al^{IV}$, $Fe_{tot}$ and Mg (in mol. %) and the calculated temperatures of formation after CHATELINEAU (1988) (I) and JOWETT (1991) (II). The biotite formulae were calculated on the basis of 7 cations. K was excluded, because its amount is often smaller than the theoretical value.

| | **Chlorite** | | | | | | | | **Biotite** | |
|---|---|---|---|---|---|---|---|---|---|---|
| $SiO_2$ | 22.32 | 21.63 | 22.18 | 22.28 | 22.48 | 23.21 | 23.58 | 23.67 | 33.62 | 33.52 |
| $TiO_2$ | 0.09 | 0.09 | 0.05 | 0.06 | 0.04 | 0.08 | 0.07 | 0.13 | 1.33 | 1.20 |
| $Al_2O_3$ | 21.09 | 21.35 | 21.75 | 21.45 | 21.93 | 20.58 | 21.09 | 21.15 | 17.43 | 17.02 |
| $FeO_{anal.}$ | 43.67 | 43.21 | 42.61 | 40.71 | 40.85 | 40.73 | 37.86 | 38.71 | 30.90 | 29.15 |
| MnO | 0.04 | 0.07 | 0.08 | 0.04 | 0.10 | 0.07 | 0.11 | 0.05 | n.d. | n.d. |
| MgO | 2.19 | 2.84 | 3.34 | 4.11 | 4.26 | 4.88 | 5.45 | 5.99 | 4.06 | 5.68 |
| CaO | n.d. | n.d. | n.d. | 0.02 | n.d. | 0.05 | n.d. | n.d. | n.d. | n.d |
| $Na_2O$ | 0.09 | 0.08 | n.d. | n.d. | n.d. | 0.05 | n.d. | n.d. | 0.16 | 0.14 |
| $K_2O$ | 0.25 | n.d. | 0.04 | n.d. | 0.10 | n.d. | 0.88 | 0.20 | 9.42 | 9.12 |
| $FeO_{calc.}$ | 42.51 | 41.26 | 41.56 | 40.29 | 40.18 | 39.99 | 37.08 | 38.54 | 30.90 | 29.15 |
| $Fe_2O_{3calc.}$ | 1.29 | 3.06 | 1.16 | 0.47 | 0.75 | 0.82 | 0.85 | 0.19 | – | – |
| $H_2O_{calc.}$ | 10.49 | 10.48 | 10.61 | 10.53 | 10.67 | 10.67 | 10.73 | 10.82 | 3.33 | 3.59 |
| Total | **100.36** | **100.86** | **100.77** | **99.25** | **100.47** | **100.40** | **99.84** | **100.74** | **100.25** | **99.42** |
| Si | 2.549 | 2.473 | 2.504 | 2.536 | 2.523 | 2.606 | 2.635 | 2.620 | 2.703 | 2.687 |
| Al | 1.451 | 1.527 | 1.496 | 1.464 | 1.477 | 1.394 | 1.365 | 1.380 | 1.297 | 1.313 |
| Σ | **4000** | **4.000** | **4.000** | **4.000** | **4.000** | **4.000** | **4.000** | **4.000** | **4.000** | **4.000** |
| Al | 1.388 | 1.351 | 1.398 | 1.414 | 1.425 | 1.329 | 1.413 | 1.381 | 0.355 | 0.295 |
| Ti | 0.008 | 0.008 | 0.004 | 0.005 | 0.003 | 0.007 | 0.006 | 0.011 | 0.081 | 0.072 |
| $Fe^{3+}$ | 0.111 | 0.186 | 0.099 | 0.040 | 0.063 | 0.069 | 0.072 | 0.016 | – | – |
| Mg | 0.373 | 0.484 | 0.563 | 0.698 | 0.713 | 0.817 | 0.907 | 0.990 | 0.486 | 0.679 |
| $Fe^{2+}$ | 4.060 | 3.946 | 3.924 | 3.836 | 3.773 | 3.754 | 3.465 | 3.569 | 2.078 | 1.954 |
| Mn | 0.004 | 0.007 | 0.007 | 0.004 | 0.009 | 0.007 | 0.011 | 0.005 | – | – |
| Ca | – | – | – | 0.003 | – | 0.006 | – | – | **3.000** | **3.000** |
| Na | 0.020 | 0.018 | – | – | – | 0.011 | – | – | 0.025 | 0.022 |
| K | 0.036 | – | 0.005 | – | 0.014 | – | 0.126 | 0.028 | 0.966 | 0.933 |
| Σ | **6.000** | **6.000** | **6.000** | **6.000** | **6.000** | **6.000** | **6.000** | **6.000** | **0.991** | **0.955** |
| OH | 8.000 | 8.000 | 8.000 | 8.000 | 8.000 | 8.000 | 8.000 | 8.000 | 1.789 | 1.919 |
| O | – | – | – | – | – | – | – | – | 0.211 | 0.081 |
| Σ | **8.000** | **8.000** | **8.000** | **8.000** | **8.000** | **8.000** | **8.000** | **8.000** | **2.000** | **2.000** |
| O | **10.000** | **10.000** | **10.000** | **10.000** | **10.000** | **10.000** | **10.000** | **10.000** | **10.000** | **10.000** |
| $Al^{VI}$ | 23.40 | 22.64 | 23.36 | 23.61 | 23.85 | 22.24 | 24.12 | 23.19 | 12.16 | 10.08 |
| $Fe_{tot}$ | 70.31 | 69.25 | 67.23 | 64.73 | 64.21 | 63.98 | 60.39 | 60.19 | 71.19 | 66.73 |
| Mg | 6.29 | 8.11 | 9.41 | 11.66 | 11.94 | 13.68 | 15.49 | 16.62 | 16.65 | 23.19 |
| I (°C) | 405.3 | 429.7 | 419.8 | 409.5 | 413.6 | 386.9 | 377.6 | 382.4 | | |
| II (°C) | 423.1 | 447.5 | 436.1 | 425.0 | 429.0 | 401.9 | 391.7 | 396.2 | | |

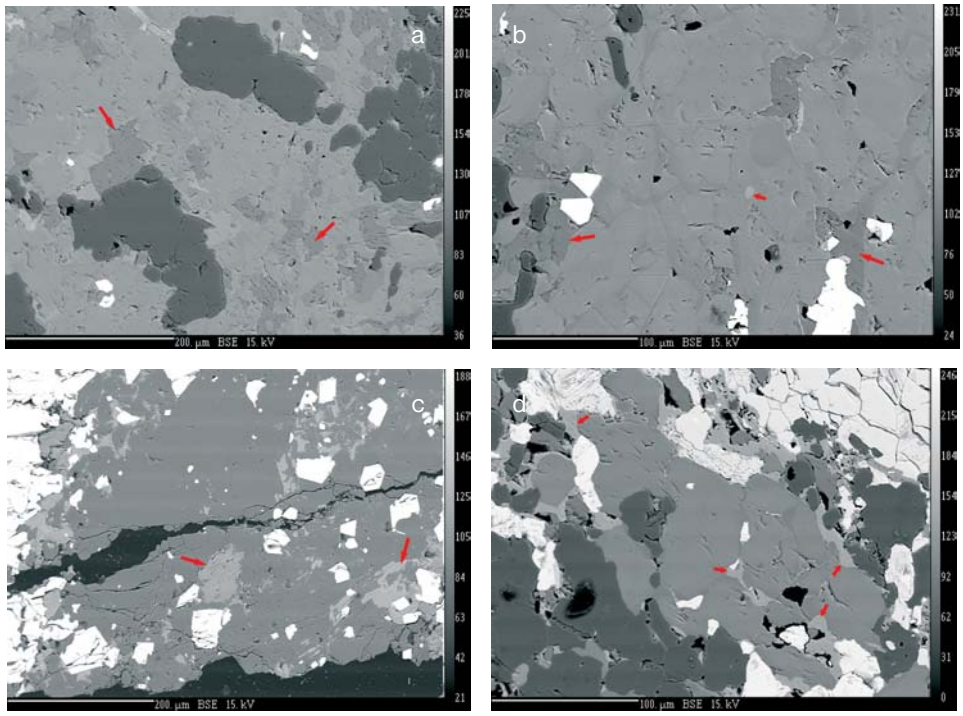


Fig. 12. BSE photographs of the ore.

a: BSE image showing zoned ankerite with inclusions of calcite (slightly darker, arrows). Quartz is black, magnetite bright. Assemblage type II, sample 861/6. Longer edge 550 µm.

b: BSE image showing strongly zoned ankerite containing an inclusion of siderite (small arrow) and inclusions of calcite (longer arrows). Magnetite is bright and quartz black. Assemblage type III, sample 861/12. Longer edge 300 µm.

c: BSE image with quartz (dark grey) having inclusions of magnetite (white) and ankerite (arrows) with corroded grain boundaries. Assemblage type I, sample 861/7. Longer edge 550 µm.

d: BSE image of quartz (dark), silicates (bright), magnetite (slightly brighter) and zoned ankerite (diagonal arranged) with siderite inclusions (arrows). Assemblage type II, sample 861/6. Longer edge 300 µm.

The composition of ankerite is similar to those of assemblage II and III. In relation to these assemblages, however, siderite has lower calcite and higher magnesite-contents in the solid solution.

The chemical composition of *magnetite* and *ilmenite* is presented in Tab. 10. Magnetite in all assemblages is almost pure end member, but it always contains small amounts of $TiO_2$ and $Al_2O_3$. Expressed in the form of the end-members, ulvite component ranges between 0.2 and 1.0 mol. % and hercynite between 0.35 and 2.25 mol. %. The composition of ilmenite is characterized by low contents of pyrophanite, geikielite and $CaTiO_3$ components which do not exceed 1 mol. %, and slightly higher hematite contents (0.6 to 3.6 mol. %). *Feldspar* from rock IV consists of $Ab_{95.7}An_{3.9}Or_{0.4}$ (calculated from an electron-microprobe analysis showing the highest CaO-content). Sporadically analysed *apatite* (analyses are not presented) does not show any Cl and F concentrations and is therefore pure hydroxylapatite.

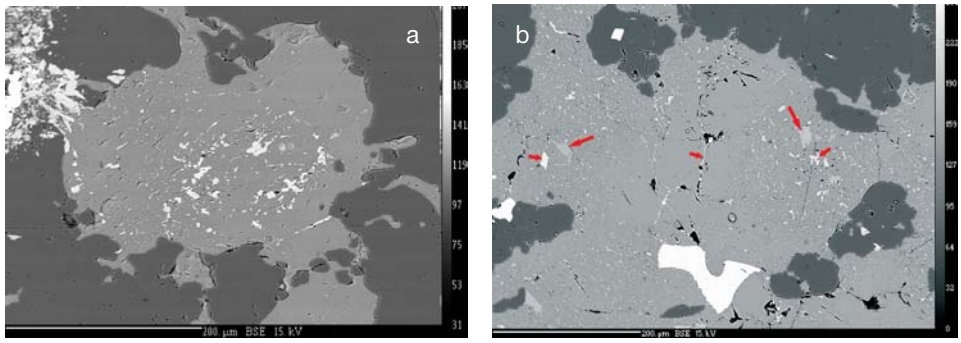


Fig. 13. BSE photographs of the ore.

a: BSE image of calcite embedded in quartz (dark). Calcite contains irregularely shaped siderite inclusions mainly occurring in the centre of the calcite crystal. Assemblage type I, sample 861/1. Longer edge 420 μm.

b: BSE image of a calcite aggregate, associated with pyrrhotite (white) and quartz (black). Calcite contains irregularly shaped siderite (highest reflecting inclusions; short arrows) and ankerite (distinctly brighter than calcite; long arrows). Siderite also occurs along grain boundaries (long arrow) of homogeneous calcite (central part). Assemblage type I, sample F/08. Longer edge 500 μm.

## 7. Discussion

### 7.1. Whole-rock chemical composition

The oxides $Fe_2O_3$, FeO, CaO and LOI occur in varying proportions (Table 1). The iron contents correlate with the relative abundances of magnetite, amphibole, chlorite, ankerite and siderite, and CaO with calcite and ankerite. The values of LOI especially reflect $CO_2$ present in carbonates (assemblage type II contains about 20 wt. % of $CO_2$ and assemblage type III about 12 wt. % $CO_2$). LOI is also connected with chlorite containing of $H_2O$ (rock type IV). The total iron concentration (expressed as $FeO_{tot}$) varies distinctly. The highest values occur in assemblage type I (45.15–47.95 wt. %) and the lowest in assemblage type II (27.10–28.98 wt. %). Assemblage type III has intermediate $FeO_{tot}$ concentrations lying between 33.62 and 40.34 wt. %. The $FeO_{tot}$ value of rock type IV is relatively high (41.48 wt. %) and, therefore close to $FeO_{tot}$ of assemblage type I.

According to the mineralogical composition and the rock microstructure, the rock type IV is a chlorite-amphibole(-magnetite-ilmenite) schist. A similar rock, characterized as chlorite schist, was analysed by Fojt *et al.* (1993) showing nearly the same element-oxide concentrations as in the above-mentioned schist [e.g. 42.64 wt. % $FeO_{tot}$ (Tab. 1, sample "Fojt")]. However, this rock has an elevated CaO-value (3.34 wt. %) as an indication for the occurrence of carbonate. Pouba and Hettler (1950) also observed chlorite schist in Malý Děd. The authors stated that this rock originated from metamorphosed mafic tuff or tuffite.

### 7.2. Rare earth elements

Striking feature of all analyses is the relatively high LREE and low HREE-content expressed by the ratio of LREE/HREE (Tab. 2). The chondrite-normalized REE patterns (Fig. 14; normalization after Anders and Grevesse 1989) are enriched in LREE. Apart from one sample (861/3) containing the highest amount of quartz and having the LREE/HREE ratio of 10.51, the ratio of the other samples varies between 4.29 and 8.52. By comparing the individual patterns three other characteristics become obvious:

1. In all assemblages the pattern shapes are similar.
2. Apart from one sample (861/4), a marked negative Eu-anomaly occurs.
3. The patterns exhibit a pronounced negative Ce-anomaly.

The decrease of the chondrite-normalized REE distribution patterns resembles basic rocks, but contains also features observed in metamorphic and crustal rocks. It is inferred that the negative Eu-anomaly ($Eu_N/Eu^*$= 0.82 – 0.51) occurring in eight of the nine samples was inherited from the basic rock material. The absence of the Eu anomaly in the sample 861/4 (assemblage type II) may be explained that it consists nearly completely of carbonate and quartz and has therefore only low magnetite and chlorite/amphibole-contents. The negative Ce-anomaly ($Ce_N/Ce^*$= 0.82 – 0.66) occurring in all samples is most probably a reflection of the influence of reducing conditions of the sea water.

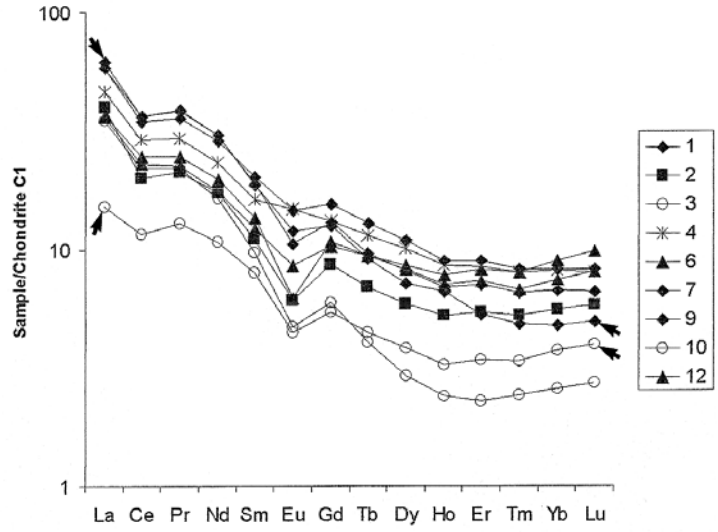


Fig. 14. Chondrite-normalized REE plots for 9 samples from assemblage type I [1, 2, 3 and 7 (arrowed)], type II (4 and 6), type III (9 and 12) and rock type IV (10, arrowed).

### 7.3. Fluid evolution

The earliest found fluid system has been trapped within Type Q1 fluid inclusions hosted by quartz. The $H_2O$-$CO_2$ inclusions belonging to this stage exhibit highly variable phase composition from members rich in $CO_2$ to members rich in $H_2O$. The phase variability is a characteristic feature for both FI in clusters and solitary. This essentially reduces the possibility of its secondary post-entrapment origin (i.e., by necking-down) and favours its primary nature. The feature may be explained by trapping of heterogeneous fluid, composed of a mechanical mixture of water- and $CO_2$-rich phases. Such an explanation may be supported also by contrasting salt content of $H_2O$- and $CO_2$-rich FI (sample MD), because salts are poorly soluble in $CO_2$-dominating fluid. Moreover, the absence of essentially pure aqueous and $CO_2$ inclusions indicate that fluid mixture would have been trapped in a high-temperature regime. Heterogeneous fluid entrapment allows specification of the PT-conditions based on fluid inclusion data only. In such situations, the minimum measured homogenization temperature represents the trapping temperatures. The corresponding homogenization pressure is equal to trapping pressure (e.g., HURAI *et al.* 2002). In our case, the appropriate PT-conditions are located at ~435 °C and ~3.5 kbars (Fig. 15) possibly reflecting the "peak" metamorphic overprint in this area.

The younger fluid type is represented by $CO_2$ fluids enclosed within abundant Type Q2 FI in quartz and P FI in ankerite. However, it seems to be unlikely that such a $CO_2$-do-

minating fluid could be the ultimate fluid phase from which the carbonate had precipitated. Therefore, it is probable that during this stage also coexist two fluids in the hydrothermal system: one rich in $CO_2$ (which was widely trapped in FI) and second rich in $H_2O$ (which was essentially not trapped in FI). There are described examples of such a selective entrapment producing fluid inclusion assemblages with essentially stable phase proportions in the literature (i.e., HEDENQUIST and HENLEY 1985, BODNAR *et al.* 1985). Nevertheless, a possible candidate to represent the water-rich endmember is fluid phase preserved in a group of secondary FI in quartz sample MD1 which exhibit only very low $CO_2$ content. It must be stressed, however, that direct evidence for such coexistence is still lacking. If this assumption is true, then the plausible PT-conditions of entrapment would be located at ~210 °C and ~1 kbar (Fig. 15).

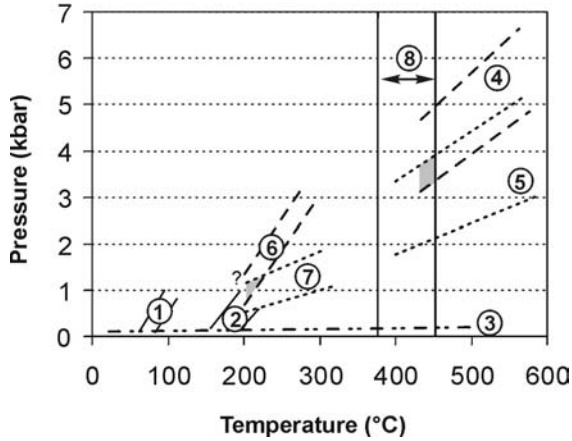


Fig. 15. Summary of available PT-data and isochores of fluid inclusions from Malý Děd. The shaded areas represent possible PT-conditions of fluid entrapment (see text).
Explanations: 1 – isochores of aqueous fluids hosted by S FI in ankerite; 2 – isochores of aqueous fluids hosted by S FI in quartz; 3 – isochores of methane fluids hosted by S FI in quartz; 4 – isochores of water-dominated $H_2O$-$CO_2$ fluids hosted by P FI in quartz (dashed line); 5 – isochores of $CO_2$-dominating $H_2O$-$CO_2$ fluids hosted by P FI in quartz (dotted line); 6 – isochores of water-dominating $H_2O$-$CO_2$ fluids in S FI in quartz; 7 – isochores of $CO_2$-dominating fluids in P FI in ankerite and S FI in quartz; 8 – chlorite compositional thermometry.

The youngest fluid systems are probably represented by aqueous fluids hosted by FI in carbonates and both aqueous and methane fluids in secondary FI in quartz. Unfortunately, their relative chronology cannot be specified due to limited information available. Most probably, these fluids may have been trapped from homogeneous fluid due to consistent phase composition of fluid inclusions. In such situation, the homogenization temperatures of aqueous inclusions are the minimum possible temperatures and the true trapping PT-conditions lie on appropriate isochores (Fig. 15). Therefore, an independent pressure or temperature estimate is required for precise location of real PT-conditions. Unfortunately, it is absent in all cases.

In conclusion, it can be stated that several different fluid systems were recognized in samples from Malý Děd, including $H_2O$-$CO_2$ mixtures, gas-free aqueous solutions and methane fluid. The position of their isochores precludes a contemporaneous generation of all fluid types. Rather, the data suggest a long lasting fluid history, covering the peak and retrograde phases of Variscan metamorphism as well as possible post-metamorphic fluid evolution. All FI-hosting mineral phases, ankerite, calcite and quartz, host different fluid inclusion assemblages. Ankerite contains in primary inclusions fluid system postdating the

quartz-hosted "peak" fluids. This may indicate (i) later ("post-peak") origin of carbonate mineralization or (ii) younger complete recrystallization of this mineral phase. The calculated $\delta^{18}O$ value of the fluid as high as +2.7 ‰ SMOW (for temperature of 210 °C and carbonate $\delta^{18}O$ of 14.4 ‰ SMOW) being close to the lower limit for "metamorphic" waters (e.g., SHEPPARD 1986) is compatible with both mentioned possibilities.

### 7.4. Minerals

*Amphibole-(I)* contains high $Ca_B$ and $(Na + K)_A$-values (Tab. 4) and, therefore, belongs to the group of calcic amphiboles. The Si-values vary from about 5.70 to about 6.25 and the $X_{Mg}$ = 0.15 or lower (Fig. 16, right side). This amphibole is identical with ferrotschermakite.

*Amphibole-(II)* has a low MgO-number [(Mg/(Mg + Fe) = about 0.25], a high $SiO_2$-number (mostly higher than 7.75) and very low CaO contents (Fig. 16, left side). Therefore, this amphibole belongs either to the monoclinic grunerite or to the orthorhombic ferroanthophyllite. Due to the intimate intergrowth of the extremely fine-grained ferroanthophyllite/grunerite with chlorite and the preponderance of the latter, X-ray diffraction analyses and optical investigations failed to determine the symmetry of amphibole.

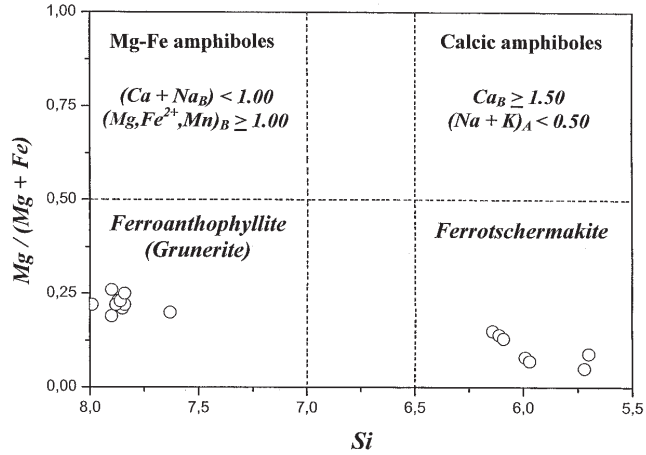


Fig. 16. Combined presentation of Fe-Mg amphiboles (left side) and calcic amphiboles (right side), the analytical points of the two investigated amphiboles (in mol. %) and their general definitions (presented in the upper parts) according to LEAKE *et al.* (1997).

According to the biotite-classification diagram of RIEDER *et al.* (1998) using the Fe-number, and the amount of $Al^{IV}$, biotite of Malý Děd is siderophyllite (Fig. 17). The plots show that the Fe and $Al^{IV}$-contents are slightly changing only. The chemical composition of chlorite corresponds to iron-rich chamosite with Si close to about 2.5 apfu and the Fe-number [$Fe_{tot}/(Fe_{tot} + Mg)$] higher than 0.75 (Fig. 18). Useful for illustrating differences in compositions of chlorites that were formed in defined environments (e. g. felsic, mafic, ultramafic) is the diagram of LIARD (1988), modified and complemented by MÜCKE (2006). This diagram, presented in Fig. 19, uses the Al/(Al + Fe + Mg) vs. Mg/(Mg + Fe) values. The chlorite plots occupy a small field only (Al numbers are about 0.4 and the Mg-numbers vary from 0.05 to 0.2) that is identical with chlorites of Algoma type iron-formations. The temperatures of formation of the chlorites were calculated according to CATHELINEAU (1988) and JOWETT (1991). The results are presented in Tab. 5 (last two lines). The temperatures vary between 378 to 430 °C (on average 403 °C of 8 analyses after CATHELINEAU) and 392 and 448 °C (on average 419 °C of 8 analyses after JOWETT).

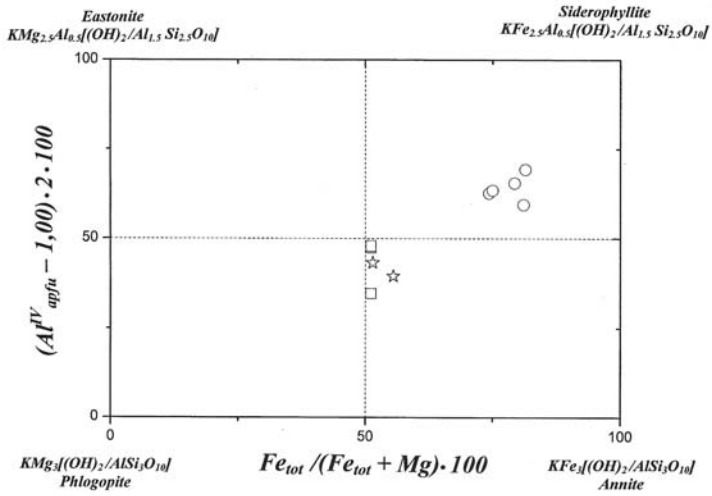


Fig. 17. Phlogopite/eastonite-annite/siderophyllite diagram of RIEDER *et al.* (1998) and the analytical plots of the investigated mica solid solutions of Malý Děd (circle) and Rejvíz-Ulrichsbrücke (square); and Seč (star).

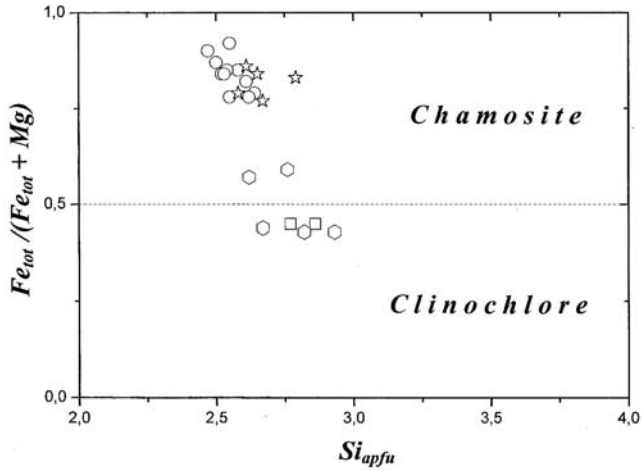


Fig. 18. Chlorite diagram in mol. % according to MELKA (1965) and the analytical plots of the investigated chlorites of Malý Děd (circle) and Rejvíz-Ulrichsbrücke (square); and of Lahn-Dill deposits south (star) and north-east of Malý Děd (hexagon).

The Figs. 17 and 18 contain additional plots obtained from other Lahn-Dill deposits of the Vrbno Group. In Fig. 17 analyses of ZIMÁK (2002b) and ŽÁČEK (2007) show that biotite of Seč (close to Jeseník) is richer in Mg (at the expense of Fe) and Si (at the expense of Al) than siderophyllite of Malý Děd and is, therefore identical with annite lying close to the phlogopite-field. Similar in composition is biotite of Rejvíz-Ulrichsbrücke (unpublished data of the authors). The chlorite-diagram of Fig. 18 contains plots of chlorite occurring either south or north-east of Malý Děd. The southern part includes the deposits of Skály (near Rýmařov) (investigated by FOJT *et al.*, 2007), Chabičov (ZIMÁK and VÁVRA, 1998) and Tvrdkov (close to Skály) (ZIMÁK 2001), Benkov (lying between Zábřeh and Rýmařov) and Králová (close to Uničov) (MELKA and VYBÍRAL, 1977). The chlorite plots of

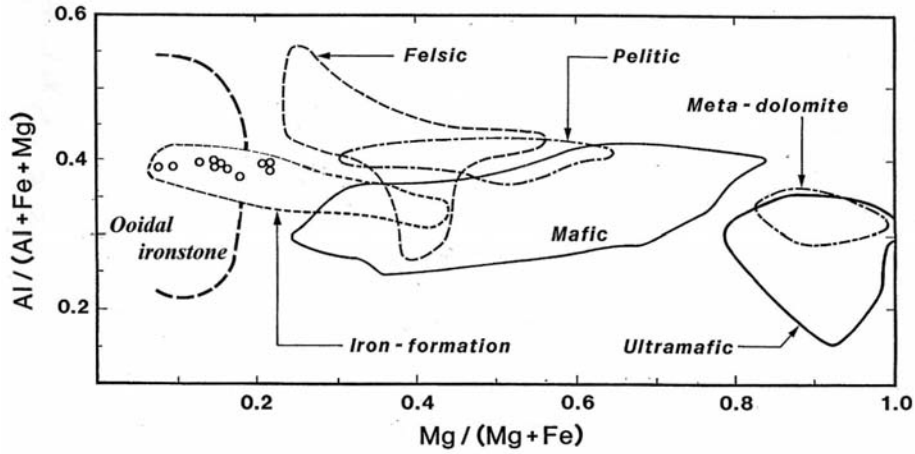


Fig. 19. Chlorite environmental classification diagram-[Mg/(Mg + Fe) vs. Al/(Al + Fe + Mg)] from LIARD (1988) modified by MÜCKE (2006) and the analytical plots of the Lahn-Dill type deposit of Malý Děd lying exactly in the field of iron-formations.

these occurrences lie exactly in the field of chlorite from Malý Děd indicating that they were formed under similar metamorphic conditions. However, chlorite plots from Mlýnský vrch, Drakov (both localities are close to Heřmanovice) and Seč analysed by ZIMÁK (2000, 2002a and 2002b) are lying in the field of Mg-rich chamosite or clinochlore. The latter was also observed in Rejvíz-Ulrichsbrücke (unpublished data of the authors). As a sign that both clinochlore and annite of the north-eastern deposits were formed under higher grade metamorphic conditions than chamosite and siderophyllite of Malý Děd, garnet occurs in Drakov (ZIMÁK, 2000) and in Rejvíz-Ulrichsbrücke (unpublised data of the authors). Garnet from Drakov consists predominantly of grossularite (67.67 mol. %) and almandine (31.28 mol. %) and from Rejvíz-Ulrichsbrücke of grossularite (48.08 mol. %) and andradite (48.40 mol. %). The relatively high Mg-concentration in both biotite and chlorite and the occurrence of garnet in deposits north-east of Malý Děd are indications that at least high-grade greenschist or even amphibolite facies conditions were attained.

The analytical data of carbonate, summarized in the Tables 6 to 9, are presented in Fig. 20. In this figure, containing analytical plots within the $FeCO_3$-$MgCO_3$-$MnCO_3$ diagram, carbonate parageneses of the assemblages I – III are summarized:

- The Fig. 20a shows analytical data of assemblage type I (containing up to 5 vol. % carbonate) in which calcite and rarely ankerite occur. Calcite containing small siderite-concentrations is the host of inclusions consisting of ankerite and siderite (Fig. 13b) or of siderite alone (Fig. 13a). Siderite contains low calcite-concentrations (below 10 mol. %) and, in relation to siderite of assemblages II and III, relatively high concentrations of $MgCO_3$, whereas ankerite is relatively rich in Fe. On the other hand, ankerite hosting calcite inclusions occurs in relatively small grains (about 50 μm; Fig. 12c) and has considerable chemical variations, whereas the composition of the calcite inclusion is nearly the same as that of the calcite-host.
- The Fig. 20b contains the plots of assemblage II that contains up to 80 vol. % carbonate. Zoned dolomite-ankerite solid solutions are the host crystals. These contain inclusions of calcite (Fig. 12a) or siderite (Fig. 12d). Siderite, mainly free of the magnesite, contains about 10 mol. % calcite, whereas calcite has only small contents of siderite (maximum 5.5 mol. %) in the solid solution.

- The Fig. 20c contains the plots of assemblage type III containing up to 25 vol. % carbonate. Zoned ankerite is the host which may contain inclusions of calcite and rarely siderite (Fig. 12b). Along the $CaMg(CO_3)_2$ – $CaFe(CO_3)_2$ join, the composition of the host is located. Similar to the other two assemblages, the composition of the solid solution varies in distinct limits, but is always dominated by the ankerite-endmember. However, the chemical variation is relatively small in ankerite which is free of inclusions. Calcite of the inclusions contains $FeCO_3$ concentrations of more than 10 mol. % (rarely more than 20 mol. %) and $MgCO_3$ concentration of slightly more than 5 mol. %. The composition of siderite of the inclusions is similar to those of assemblage II.

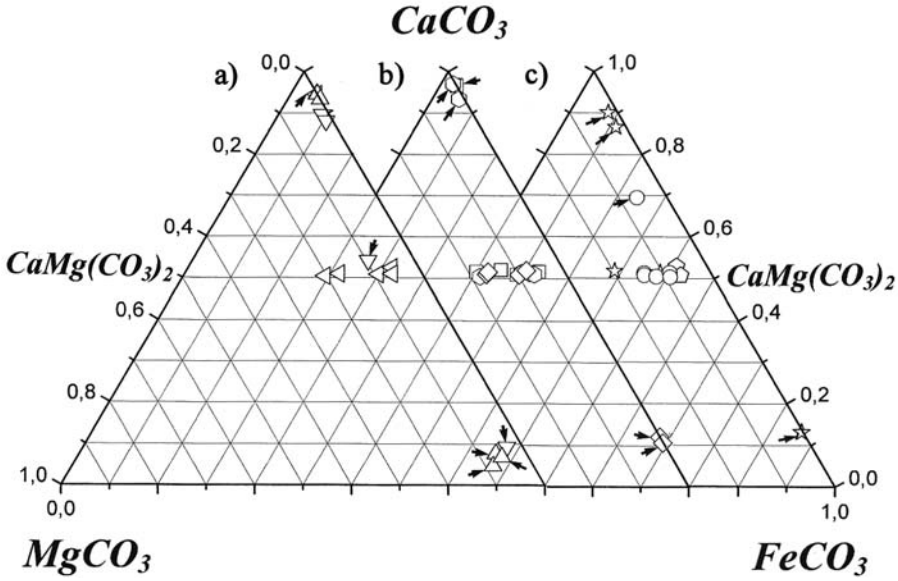


Fig. 20. $MgCO_3$-$FeCO_3$-$CaCO_3$ diagrams containing analytical plots of a) assemblage I that consists of calcite and rarely ankerite. Calcite (host) has inclusions of siderite (arrows) or siderite and ankerite (arrows); b) assemblage II that consist of zoned ankerite (host) having inclusions of siderite (arrows) and calcite (arrows); c) assemblage III that consists of ankerite alone or of ankerite (host) having inclusions of calcite (arrows) and siderite (arrow).

In most of the carbonate parageneses of the assemblages II and III, the host is zoned dolomite-rich ankerite. It contains inclusions of calcite and siderite. Calcite is intimately intergrown with the host (Fig. 12a) and siderite occurs not only in the centre of the host crystals, but also along their rim (Fig. 12d). Therefore it is inferred that host and inclusion were formed almost together and are of the same age. However, in assemblage I in which calcite is the host, the inclusions are corroded and irregularly distributed. The inclusions consist of siderite only (Fig. 13a) or of siderite + ankerite (Fig. 13b). In the central part of Fig. 13b, the inclusions have been expelled from the host probably due to re-equilibration during metamorphism and siderite occurs along grain boundaries. These textures resemble features related to decomposition, agreeing with investigations in the system $CaCO_3$-$FeCO_3$ of GOLDSMITH *et al.* (1962) and ROSENBERG (1963). This diagram contains a considerable miscibility gap. The gap becomes smaller with increasing temperature especially in the area of calcite-rich solid solutions, containing high $FeCO_3$-concentrations (generally lying between 2.48 and 11.20 mol. %, but exceptionally up to 24.19 mol. %). Therefore, it is inferred that the calcite-siderite solid solutions of our study were formed close to, but not higher than a temperature of 450 °C. With decreasing temperature during cooling, the calcite-siderite solid solution became unstable and decomposed into calcite with lower siderite content

Table 6. Ankerite, calcite and siderite analyses of assemblage type II in wt. % (upper part) and in end-member concentration (mol. %, lower part). Ankerite-dolomite is also presented identical to the calcite-group in mol. %. Ankerite analyses I, II, VII and VIII are from the rim and III, IV, IX and X from the core of the zoned ankerite crystals. I (without index: rim of the crystal), IIc (core of the crystal). The formulae of carbonate were calculated on the basis of 1 cation (calcite-group) and 2 cations (dolomite-group), respectively.

| | **Assemblage II** | | | | | | | | | | | |
|---|---|---|---|---|---|---|---|---|---|---|---|---|
| | **861/6: zoned Ankerite + Calcite** | | | | | | **861/6: zoned Ankerite + Siderite** | | | | | |
| | **I** | **II** | **$III_c$** | **$IV_c$** | **V** | **VI** | **VII** | **VIII** | **$IX_c$** | **$X_c$** | **XI** | **XII** |
| FeO | 21.04 | 24.17 | 25.96 | 29.31 | 2.25 | 2.48 | 22.61 | 22.79 | 26.74 | 27.16 | 55.11 | 55.07 |
| MnO | 0.72 | 0.53 | 0.42 | 0.25 | 0.20 | 0.15 | 0.65 | 0.62 | 0.45 | 0.31 | 0.22 | 0.28 |
| MgO | 7.18 | 5.01 | 3.88 | 2.03 | n.d. | n.d. | 6.28 | 6.23 | 3.77 | 2.96 | 0.02 | 0.05 |
| CaO | 28.11 | 27.95 | 27.33 | 27.45 | 54.10 | 53.92 | 26.99 | 28.06 | 27.02 | 27.30 | 5.87 | 5.11 |
| SrO | 0.04 | n.a. | 0.11 | 0.08 | 0.12 | 0.17 | 0.08 | 0.02 | 0.03 | 0.07 | 0.06 | n.d. |
| $CO_{2calc.}$ | 43.24 | 42.54 | 41.26 | 41.91 | 44.01 | 44.00 | 43.03 | 43.17 | 41.99 | 41.51 | 38.55 | 37.97 |
| Total | **100.33** | **99.20** | **98.96** | **101.03** | **100.68** | **100.72** | **100.47** | **100.89** | **100.00** | **99.31** | **99.83** | **98.48** |
| $FeCa(CO_3)_2$ | 56.90 | 69.60 | 77.06 | 85.70 | – | – | 64.38 | 64.68 | 78.02 | 80.14 | – | – |
| $MnCa(CO_3)_2$ | 2.06 | 1.56 | 1.26 | 0.74 | – | – | 1.88 | 1.74 | 1.34 | 0.94 | – | – |
| $MgCa(CO_3)_2$ | 36.26 | 25.72 | 20.52 | 10.58 | – | – | 32.68 | 31.50 | 19.62 | 15.56 | – | – |
| $SrCa(CO_3)_2$ | 0.08 | – | 0.24 | 0.16 | – | – | 0.16 | 0.04 | 0.06 | 0.14 | – | – |
| $CaCa(CO_3)_2$ | 2.00 | 3.12 | 0.92 | 2.82 | – | – | 0.90 | 2.04 | 0.96 | 3.22 | – | – |
| $FeCO_3$ | 29.80 | 34.80 | 38.53 | 42.85 | 3.13 | 3.45 | 32.19 | 32.34 | 39.01 | 40.07 | 87.56 | 88.85 |
| $MnCO_3$ | 1.03 | 0.78 | 0.63 | 0.37 | 0.28 | 0.21 | 0.94 | 0.87 | 0.67 | 0.47 | 0.36 | 0.45 |
| $MgCO_3$ | 18.13 | 12.86 | 10.26 | 5.29 | – | – | 16.34 | 15.75 | 9.81 | 7.78 | 0.06 | 0.14 |
| $CaCO_3$ | 51.00 | 51.56 | 50.46 | 51.41 | 96.47 | 96.18 | 50.45 | 51.02 | 50.48 | 51.61 | 11.95 | 10.56 |
| $SrCO_3$ | 0.04 | – | 0.12 | 0.08 | 0.12 | 0.16 | 0.08 | 0.02 | 0.03 | 0.07 | 0.07 | – |

Table 7. Ankerite and calcite analyses of assemblages type II and I in wt. % (upper part) and in end-member concentration (mol. %, lower part). Ankerite-dolomite is also presented identical to the calcite-group in mol. %. Ankerite analyses I, VII and VIII are from the rim and II, III, IV, IX, X and XI from the core of the zoned ankerite crystals.

| | **Assemblage II** | | | | | | **Assemblage I** | | | | | |
|---|---|---|---|---|---|---|---|---|---|---|---|---|
| | **861/4: zoned Ankerite + Calcite** | | | | | | **861/7: zoned Ankerite + Calcite** | | | | | |
| | **I** | **$II_c$** | **$III_c$** | **$IV_c$** | **V** | **VI** | **VII** | **VIII** | **$IX_c$** | **$X_c$** | **$XI_c$** | **XII** |
| FeO | 21.77 | 26.80 | 27.74 | 28.81 | 1.81 | 3.93 | 20.36 | 22.26 | 27.44 | 27.85 | 28.32 | 3.81 |
| MnO | 0.53 | 0.31 | 0.28 | 0.24 | 0.19 | 0.26 | 0.55 | 0.59 | 0.28 | 0.23 | 0.15 | 0.20 |
| MgO | 7.07 | 3.43 | 2.84 | 2.46 | 54.10 | 0.45 | 7.97 | 6.70 | 3.53 | 2.04 | 2.29 | 0.05 |
| CaO | 27.28 | 27.20 | 26.86 | 26.35 | 0.19 | 52.12 | 27.85 | 27.71 | 27.21 | 27.14 | 26.28 | 53.18 |
| SrO | n. a. | n.a. | 0.05 | 0.11 | 0.10 | n.a. | 0.08 | 0.08 | 0.04 | 0.04 | 0.08 | n.a. |
| $CO_{2calc.}$ | 42.79 | 41.70 | 41.37 | 40.78 | 43.95 | 43.97 | 43.41 | 43.09 | 42.20 | 40.74 | 40.60 | 44.24 |
| Total | **99.44** | **99.44** | **99.09** | **98.64** | **100.34** | **100.73** | **100.22** | **100.43** | **99.70** | **98.04** | **98.72** | **101.48** |
| $FeCa(CO_3)_2$ | 62.32 | 78.74 | 82.14 | 84.44 | – | – | 57.46 | 63.28 | 79.64 | 83.74 | 85.46 | – |
| $MnCa(CO_3)_2$ | 1.54 | 0.92 | 0.84 | 0.74 | – | – | 1.58 | 1.70 | 0.82 | 0.70 | 0.46 | – |
| $MgCa(CO_3)_2$ | 36.08 | 17.78 | 15.00 | 13.16 | – | – | 40.10 | 33.94 | 18.26 | 10.94 | 12.34 | – |
| $SrCa(CO_3)_2$ | – | – | 0.10 | 0.24 | – | – | 0.16 | 0.16 | 0.08 | 0.08 | 0.18 | – |
| $CaCa(CO_3)_2$ | 0.06 | 2.38 | 1.92 | 1.42 | – | – | 0.70 | 0.92 | 1.20 | 4.54 | 1.56 | – |
| $FeCO_3$ | 31.16 | 39.37 | 41.07 | 42.22 | 2.52 | 5.48 | 28.97 | 31.64 | 39.82 | 41.87 | 42.73 | 5.27 |
| $MnCO_3$ | 0.77 | 0.46 | 0.42 | 0.37 | 0.27 | 0.37 | 0.80 | 0.85 | 0.41 | 0.35 | 0.23 | 0.28 |
| $MgCO_3$ | 18.04 | 8.98 | 7.50 | 6.58 | 0.49 | 1.12 | 20.21 | 16.97 | 9.13 | 5.47 | 6.17 | 0.12 |
| $CaCO_3$ | 50.03 | 51.19 | 50.96 | 50.71 | 96.62 | 93.03 | 49.94 | 50.46 | 50.60 | 52.27 | 50.78 | 94.33 |
| $SrCO_3$ | – | – | 0.05 | 0.12 | 0.10 | – | 0.08 | 0.08 | 0.04 | 0.04 | 0.09 | – |

Table 8. Calcite, siderite and ankerite analyses of assemblages type I and III in wt. % (upper part) and in end-member concentration (in mol. %, lower part). Ankerite-dolomite is also presented identical to the calcite-group in mol. %.

| | Assemblage I | | | | | | | | | | Assemb. III | |
|---|---|---|---|---|---|---|---|---|---|---|---|---|
| | 861/1: Calcite + Siderite | | | | | | F/08: Calcite + Ank + Sid | | | | 861/9 Ank | |
| | I | II | III | IV | V | VI | VII | VIII | IX | X | XI | XII |
| FeO | 3.76 | 3.85 | 4.43 | 53.67 | 54.42 | 54.04 | 6.31 | 7.35 | 24.55 | 54.62 | 27.67 | 28.78 |
| MnO | 0.35 | 0.17 | 0.36 | 0.54 | 0.79 | 1.28 | 0.21 | 0.24 | 0.42 | 0.34 | 0.35 | 0.29 |
| MgO | n.d. | n.d. | n.d. | 2.24 | 2.94 | 1.89 | 0.57 | 0.55 | 3.66 | 1.16 | 2.43 | 2.50 |
| CaO | 51.85 | 52.48 | 51.47 | 3.76 | 2.28 | 3.31 | 49.13 | 48.06 | 28.55 | 4.52 | 27.98 | 26.69 |
| SrO | 0.27 | 0.48 | 0.30 | n.d. | n.d. | n.d. | 0.11 | 0.14 | 0.12 | 0.05 | n.a. | n.a. |
| $CO_{2calc.}$ | 43.32 | 43.85 | 43.46 | 38.61 | 38.82 | 38.56 | 43.22 | 43.03 | 41.75 | 38.50 | 41.77 | 41.49 |
| Total | **99.55** | **100.85** | **100.02** | **98.82** | **100.04** | **99.08** | **99.55** | **99.37** | **99.05** | **99.19** | **100.20** | **99.75** |
| $FeCa(CO_3)_2$ | – | – | – | – | – | – | – | – | 72.04 | – | 81.14 | 84.98 |
| $MnCa(CO_3)_2$ | – | – | – | – | – | – | – | – | 1.24 | – | 1.04 | 0.88 |
| $MgCa(CO_3)_2$ | – | – | – | – | – | – | – | – | 19.14 | – | 12.68 | 13.14 |
| $SrCa(CO_3)_2$ | – | – | – | – | – | – | – | – | 0.26 | – | – | – |
| $CaCa(CO_3)_2$ | – | – | – | – | – | – | – | – | 7.32 | – | 5.14 | 1.00 |
| $FeCO_3$ | 5.31 | 5.38 | 6.25 | 85.16 | 85.86 | 85.86 | 8.94 | 10.46 | 36.02 | 86.89 | 40.57 | 42.49 |
| $MnCO_3$ | 0.50 | 0.24 | 0.52 | 0.86 | 1.26 | 2.05 | 0.31 | 0.35 | 0.62 | 0.55 | 0.52 | 0.44 |
| $MgCO_3$ | – | – | – | 6.34 | 8.27 | 5.35 | 1.44 | 1.39 | 9.57 | 3.29 | 6.34 | 6.57 |
| $CaCO_3$ | 93.93 | 93.92 | 92.94 | 7.64 | 4.61 | 6.74 | 89.20 | 87.66 | 53.66 | 9.21 | 52.57 | 50.50 |
| $SrCO_3$ | 0.26 | 0.46 | 0.29 | – | – | – | 0.11 | 0.14 | 0.13 | 0.06 | – | – |

Table 9. Ankerite, calcite and siderite analyses of assemblage type III in wt. % (upper part) and mol. % (lower part) and in end-member concentration (in mol. %, lower part). Ankerite-dolomite is also presented identical to the calcite-group in mol. %. Ankerite analyses I, II and VII are from the rim and III, IV, V and VIII from the core of the zoned ankerite crystals.

| | Assemblage III | | | | | | | | | | | |
|---|---|---|---|---|---|---|---|---|---|---|---|---|
| | 861/12: zoned Ankerite + Calcite | | | | | | 861/12: zoned Ankerite + Siderite + Calcite | | | | | |
| | I | II | $III_c$ | $IV_c$ | $V_c$ | VI | VII | $VIII_c$ | IX | X | XI | XII |
| FeO | 24.05 | 24.03 | 25.99 | 27.14 | 27.69 | 16.74 | 20.06 | 25.95 | 53.71 | 53.94 | 5.65 | 8.01 |
| MnO | 0.41 | 0.60 | 0.24 | 0.37 | 0.23 | 0.20 | 0.72 | 0.47 | 0.73 | 0.31 | 0.45 | 0.66 |
| MgO | 5.38 | 5.37 | 4.55 | 3.25 | 3.41 | 2.39 | 7.75 | 4.00 | 0.15 | 0.09 | 0.77 | 0.86 |
| CaO | 27.54 | 26.95 | 27.06 | 27.09 | 26.62 | 37.39 | 28.30 | 27.28 | 6.40 | 6.41 | 49.69 | 47.87 |
| SrO | 0.03 | 0.06 | 0.24 | 0.04 | 0.06 | 0.16 | 0.03 | 0.04 | 0.04 | n.d. | 0.13 | n.a. |
| $CO_{2calc.}$ | 42.48 | 41.95 | 42.37 | 41.69 | 41.74 | 42.39 | 43.42 | 41.97 | 38.56 | 38.36 | 43.63 | 43.82 |
| Total | **99.89** | **98.96** | **100.45** | **99.58** | **99.75** | **99.27** | **100.28** | **99.71** | **99.59** | **99.11** | **100.32** | **101.22** |
| $FeCa(CO_3)_2$ | 69.36 | 69.88 | 75.14 | 79.78 | 81.28 | – | 56.60 | 75.74 | – | – | – | – |
| $MnCa(CO_3)_2$ | 1.18 | 1.76 | 0.70 | 1.10 | 0.68 | – | 2.06 | 1.40 | – | – | – | – |
| $MgCa(CO_3)_2$ | 27.62 | 27.84 | 23.46 | 17.02 | 17.82 | – | 38.96 | 20.78 | – | – | – | – |
| $SrCa(CO_3)_2$ | 0.06 | 0.12 | 0.48 | 0.08 | 0.12 | – | 0.06 | 0.08 | – | – | – | – |
| $CaCa(CO_3)_2$ | 1.78 | 0.40 | 0.22 | 2.02 | 0.10 | – | 2.32 | 2.00 | – | – | – | – |
| $FeCO_3$ | 34.68 | 34.94 | 37.57 | 39.89 | 40.64 | 24.19 | 28.30 | 37.87 | 85.33 | 86.13 | 7.93 | 11.20 |
| $MnCO_3$ | 0.59 | 0.88 | 0.35 | 0.55 | 0.34 | 0.29 | 1.03 | 0.70 | 1.18 | 0.51 | 0.64 | 0.93 |
| $MgCO_3$ | 13.81 | 13.92 | 11.73 | 8.51 | 8.91 | 6.16 | 19.48 | 10.39 | 0.42 | 0.25 | 1.92 | 2.14 |
| $CaCO_3$ | 50.89 | 50.20 | 50.11 | 51.01 | 50.05 | 69.20 | 51.16 | 51.00 | 13.02 | 13.11 | 89.38 | 85.73 |
| $SrCO_3$ | 0.03 | 0.06 | 0.24 | 0.04 | 0.06 | 0.16 | 0.03 | 0.04 | 0.05 | – | – | – |

and newly-formed siderite with low calcite content. Newly-formed siderite may be associated with ankerite (Fig. 13b). According to REEDER (1983), however, the join $CaCO_3$-$FeCO_3$ does not display a dolomite (ankerite)-like component. Therefore, high temperature calcite with ankerite of decomposition origin, is firstly reported in this paper.

Table 10. Selected analyses of magnetite of assemblages I – III and rock type IV and ilmenite of rock type IV in wt. % (upper part) and in end-member concentration (in mol. %, lower part). The formulae were calculated on the basis of 3 (magnetite) and 1 cation(s), respectively.
nd = not detected.

| | **Magnetite solid solutions** | | | | | | | | | | **Ilmenite solid solutions** | | | |
|---|---|---|---|---|---|---|---|---|---|---|---|---|---|---|
| | Assemblage I | | Assemblage III | | Ass. II | Rock type IV | | | | | Rock type IV | | | |
| | **I** | **II** | **III** | **IV** | **V** | **VI** | **VII** | **VIII** | **IX** | | **X** | **XI** | **XII** | **XIII** |
| $TiO_2$ | 0.34 | 0.15 | 0.24 | 0.08 | 0.17 | 0.11 | 0.15 | 0.29 | 0.31 | | 50.69 | 51.02 | 51.88 | 51.24 |
| $Al_2O_3$ | 0.19 | 0.45 | 0.38 | 0.06 | 0.26 | 0.65 | 0.16 | 0.27 | 0.25 | | n.d. | n.d. | n.d. | n.d. |
| $FeO_{anal.}$ | 92.92 | 92.46 | 93.54 | 93.80 | 92.41 | 92.66 | 91.85 | 92.77 | 93.10 | | 48.21 | 47.81 | 47.06 | 47.50 |
| MnO | n.d. | n.d. | n.d. | n.d. | 0.05 | n.d. | n.d. | n.d. | n.d. | | 0.22 | 0.19 | 0.20 | 0.20 |
| MgO | n.d. | n.d. | n.d. | n.d. | n.d. | n.d. | 0.10 | n.d. | 0.03 | | 0.18 | 0.05 | n.d. | 0.23 |
| CaO | n.d. | n.d. | n.d. | n.d. | n.d. | n.d. | n.d. | n.d. | n.d. | | 0.21 | n.d. | n.d. | 0.07 |
| $FeO_{calc.}$ | 31.47 | 31.08 | 31.65 | 31.38 | 30.08 | 31.48 | 30.73 | 31.38 | 31.48 | | 44.80 | 45.56 | 46.50 | 45.43 |
| $Fe_2O_{3calc.}$ | 68.29 | 68.22 | 68.78 | 69.37 | 68.16 | 67.99 | 67.93 | 68.23 | 68.48 | | 3.79 | 2.51 | 0.63 | 2.30 |
| | **100.29** | **99.90** | **101.05** | **100.89** | **99.72** | **99.54** | **99.07** | **100.17** | **100.55** | | **99.89** | **99.33** | **99.21** | **99.47** |
| Ulvite | 1.0 | 0.2 | 0.7 | 0.2 | 0.5 | 0.3 | 0.4 | 0.8 | 0.9 | Pyrophanite | 0.5 | 0.4 | 0.4 | 0.4 |
| Jacobsite | – | – | – | – | 0.2 | – | – | – | – | Geikielite | 0.7 | 0.2 | – | 0.8 |
| Hercynite | 0.40 | 1.0 | 0.85 | 1.15 | 0.6 | 2.25 | 0.35 | 0.6 | 0.55 | $CaTiO_3$ | 0.6 | – | – | 0.2 |
| Spinel | – | – | – | – | – | – | 0.6 | – | 0.2 | Hematite | 3.6 | 2.4 | 0.6 | 2.2 |
| Magnetite | 98.6 | 98.8 | 98.45 | 99.65 | 98.70 | 97.45 | 98.65 | 98.6 | 98.35 | Ilmenite | 94.6 | 97.0 | 99.0 | 96.4 |

Solid solutions of ankerite-dolomite show a limited solubility. Following the studies of GOLDSMITH *et al.* (1962) and ROSENBERG (1967), REEDER (1983) stated that natural and synthetic dolomite does not contain more than roughly 70 mol. % ankerite in the solid solution. However, our results show the highest Fe-content substituting for Mg in natural dolomite to form ankerite. This is illustrated in Fig. 21, where 27 ankerite-dolomite analyses, contained in the Tables 6 to 9, are summarized. Due to their low $CaMn(CO_3)_2$ concentration (max. 2.06 mol. %), the analytical plots lie close to the $CaMg(CO_3)_2$ – $CaFe(CO_3)_2$ join and cover over a span of 38.96 dolomite/56.60 ankerite to 10.58 dolomite/85.70 ankerite solid solutions.

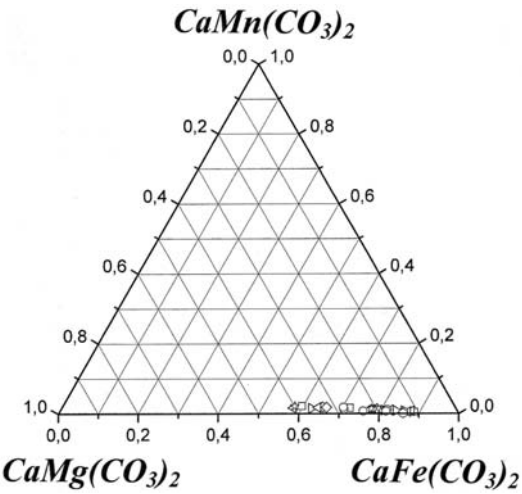


Fig. 21. Carbonate compositions in the system $CaFe(CO_3)_2$ – $CaMg(CO_3)_2$ – $CaMn(CO_3)_2$ of assemblage types I to III (mol. %) calculated from ankerite analyses contained in Tabs. 6 to 9.

The reason for this high ankerite-concentration in our carbonate solid solutions is not known to us and cannot be solved in this paper, the more so as the cause of the instability of $CaFe(CO_3)_2$ and the limited substitution of $Fe^{2+}$ for Mg in the dolomite structure had been often considered and reconsidered by various authors using various methods (e.g. ROSENBERG, 1991, REEDER and DOLLASE, 1991 and CHAI and NAVROTZKY, 1996) but left unresolved.

At high temperature, ankerite is expected to undergo a disordering transition to the calcite structure (REEDER and DOLLASE, 1991). Therefore, it may be inferred that ankerite of our study represents a disordered phase. Such a calcite-type disordered $CaFe(CO_3)_2$ phase was synthesized at 845 °C and 30 kbar by DAVIDSON *et al.* (1993). However, these PT-conditions cannot be applied to our rocks as they are by far too high. Moreover, the synthesis of DAVIDSON *et al.* (1993) concerns the ideal end-member $CaFe(CO_3)_2$ only, but not compounds of $Ca(Fe,Mg)(CO_3)_2$ containing Mg in the range of 10.38 to 38.96 mol. % as detected in our study.

*Quartz* occurs most probably in two generations. One generation is of minor abundance and occurs in irregular distribution mostly in the form of euhedral crystals or small aggregates (Figs. 12a, b, d). Apart from rock type IV, the second generation is widely distributed in all of the assemblage types and locally makes up to 30 vol. % (Fig. 5) and is either arranged parallel to the schistosity (Figs. 3 and 5) or is irregularly distributed (Fig. 4). Predominantly it replaces not only amphibole (Fig. 9b), chlorite (Fig. 7c) and carbonate (Figs. 9a), but also apatite (Fig. 9b) and rarely magnetite (Fig. 7c). The second quartz generation may be identical with silicification caused by submarine hydrothermal and exhalative activity. Silicification was accompanied by other rock alterations such as chloritization and carbonatization (MIXA and OREL, 1990).

## 8. Genesis

The Mid-European iron ores of the Devonian Lahn-Dill type (defined by AHLBURG 1911) represent a clear example of iron ore accumulation in a rift setting (QUADE 1976) that are closely associated with basaltic volcanics (SAWKINS 1990). Older considerations about the genesis of this deposit type favoured an iron- rich source identical with submarine volcanogenic exhalations. Postulated by HENTSCHEL (1960) and RÖSLER (1964) and later confirmed by LEHMANN (1972), SAWKINS and BURKE (1980), FLICK and BEHNISCH (1990) and LIPPERT and FLICK (1998) the basaltic volcanites are considered to be the source rocks of the iron deposits. These rocks were transformed during spilitization into diabase (FLICK and BENISCH 1990, NESBOR *et al.* 1993) under the release Fe and Si which were concentrated in the ore body.

Similar to the geological situation of the Lahn-Dill area in the Devonian, the study area suffered a period of extension associated with the formation of the Moravo-Silesian basin. The emplaced volcanic rocks, later transformed into metavolcanics range from arc and back-arc within plate volcanites to oceanic tholeiites with transitions to the continental tholeiites associated with rift zones (KALVODA *et al.* 2008). Our whole-rock and trace element data suggest that the chlorite-amphibole schist (rock type IV) could be a basaltic volcanite. The latter is inferred to be the source rock. This rock has a high Fe-concentration showing about 42 wt. % $FeO_{tot}$ in the whole-rock composition. The high Fe-content is a reflection of the composition of ferrotschermakite which contains nearly 40 wt. % $FeO_{tot}$. Ferrotschermakite occurring in the form of remnants in newly-formed ferroanthophyllite/grunerite or chamosite (Fig. 11a) is a primary constituent of the basaltic source rock.

Different to the Lahn-Dill area and the Harz Mountains where the iron-mineralizations originated from spilitization of the source rock, the protoliths of the iron-mineralizations of Malý Děd were formed by the interaction of two sources:

1. Submarine volcanogenic exhalations. These exhalations are rich in Fe and $CO_2$ and very low in Mn. In contact with sea water and reducing conditions $FeCO_3$ (and $MnCO_3$) precipitation occurs. Due to the elevated $CO_2$-concentrations, the normal sea water precipitation increases and as a consequence $FeCO_3$ (+ $MnCO_3$) occur together with $CaCO_3$ and $MgCO_3$. The influence of the marine environment is documented by the occurrence of Sr in nearly all carbonate analyses (Tabs. 6 to 9) ranging from 0.03 to 0.48 wt. % SrO and in the whole-rock chemical analyses of the carbonate-bearing ore (e.g. assemblage type II has Sr-contents lying between 298 and 226 ppm).
2. Submarine pyroclastic material. It is fine-grained like ashes, had the same or a similar chemical composition as the source rock and, therefore the same high Fe-concentration. Within the deposit of Malý Děd, the pyroclastic material may be chemically identical with chlorite-schist that originated according to Pouba and Hettler (1950) from basic tuff or tuffite.

From these two sources, differently composed sediments originated that were deposited in the form of layers in the marine basin:

- In phases of strong volcanogenic-exhalative activity (or low input of pyroclastics) the sediments are dominated by carbonate precipitations identical with the protolith of assemblage type II.
- In phases of absent or strongly reduced volcanogenic-exhalative activity (or high input of pyroclastics) the amount of carbonate is low and the resulting sediments are identical with the protolith of assemblage type I.
- In phases in which both, the volcanogenic-exhalative activity and the input of pyroclastics are moderate, the sedimentation of the protolith of assemblage type III occurs.

Caused by metamorphic events of the Variscan orogeny (Schulmann and Gayer 2000), the basaltic volcanite was transformed into chlorite-amphibole schist. Deduced from prevailing rock patterns, ferrotschermakite transformed into ferroanthophyllite/grunerite which recrystallized into the crenulation-cleavage texture (Figs. 10a, b). Similar to ferroanthophyllite, quartz (Fig. 10a), ilmenite (Fig. 11b) and graphite suffered the same metamorphic overprint as they are arranged in the same texture. Chamosite is younger and inferred to be of retrograde origin. This is supported by the fact that chamosite forms pseudomorphic replacement textures after ferroanthophyllite/grunerite only, mostly inheriting the pre-existing crenulation-cleavage texture (Figs. 10c, d).

The same Variscan metamorphism transformed the pyroclastic material into mixtures of amphibole, exceptionally biotite, magnetite and quartz and the precipitations of carbonates into siderite-bearing calcite and dolomite-rich ankerite. Under retrograde conditions, amphibole and biotite were mostly replaced by chamosite. The second quartz generation is inferred to be formed under the same metamorphic conditions. The conditions of the high-grade greenschist facies are marked by the appearance of biotite and the elimination of dolomite-ankerite (in the presence of quartz), which is stable under low-grade conditions of the greenschist facies only. However, both biotite and ankerite-dolomite occur in the ore body of Malý Děd. In relation to the abundance of ankerite-dolomite (locally up to 80 vol. %), the amount of biotite is negligible low obtaining not more than 1 vol. %. From these relationships it is concluded that the rocks were formed just at the border between low-grade to high-grade conditions of the greenschist facies. According to Matthes (1983), the temperature of the greenschist facies varies approximately between 400 °C (2–5 kbar $PH_2O$) and 450–470 °C (under a medium geothermal gradient and a corresponding gas pressure

and a medium $CO_2/H_2O$-ratio). The calculated temperatures derived from the chlorite geothermometers of CATHELINEAU (1988) and JOWETT (1991) lying on average at 403 °C and 419 °C, the temperature of close to 450 °C obtained from considerations within the $CaCO_3$-$FeCO_3$ system and from trapping of the early "peak" $CO_2$-$H_2O$ fluid inclusions leading to ~ 450 °C and ~ 3.5 kbars, fit well into the results of our petrographic considerations.

The ore body of Malý Děd may contain pyrrhotite (Fig. 7d). Various authors assume that iron sulphides precipitated from the sea water containing $Fe^{2+}$ and $S^{2-}$ -ions. The latter are considered to have been derived from bacterial reduction of marine sulphate. SAWLOWICZ (1989) reported the $\delta^{34}S$-values of sulphides resulting from bacterial sulphate reduction in the "Kupferschiefer" between –40 and –25‰ CDT (on average –35‰ CDT). However, the $\delta^{34}S$ values, established by FOJT *et al.* (1993) lie in the range between –14.6 and –19.6‰ CDT and seem to be too heavy to represent a "bacterial" source. HLADÍKOVÁ and KŘIBEK (1988) reported $\delta^{34}S$ values around –15 and 0‰ CDT, similar to those obtained by FOJT *et al.* (1993) and inferred that sulphur was leached from associated rocks such as schists and basic metavolcanites.

## 9. Conclusion

Malý Děd is one of about 40 iron mineralizations within the Vrbno Group. On a genetic point of view all these are identical, because they belong to the Lahn-Dill type. However, on a mineralogical point of view they are different, caused by varying conditions of metamorphic changes under which the protolith of the iron mineralizations was transformed. The minerals (chamosite: Fe/(Fe + Mg) from 0.78 to 0.92; siderophyllite: Fe/(Fe + Mg) from 0.74 to 0.83) of Malý Děd originated just at the border between low-grade to high-grade conditions of the greenschist facies. The deposits north-east of Malý Děd underwent conditions of the high-grade greenschist or even the amphibolite facies; this was deduced from lower Fe-concentrations in chlorite (= clinochlore/chamosite: Fe/(Fe + Mg) from 0.44 to 0.59) and biotite (= annite: Fe/(Fe + Mg) from 0.51 to 0.56) and the occurrence of garnet (grossularite-almandine or grossularite-andradite solid solutions). On the other hand, the deposits in the southern part of the Vrbno Group contain chlorite (= chamosite: Fe/(Fe + Mg) from 0.77 to 0.86) which is identical in composition with chlorite of Malý Děd. Therefore, it was inferred that these deposits had suffered similar metamorphic changes. However, the occurrence of stilpnomelane, greenalite and minnesotaite (e. g. MELKA and VYBÍRAL, 1977; ZIMÁK and VÁVRA, 1998; ZIMÁK, 2001; and FOJT *et al.*, 2007) in the southern deposits are indications for distinctly lower-grade metamorphic conditions as discussed for Malý Děd.

## Acknowledgements

Electron-microprobe analyses were carried out at the Institut für Endlagerforschung of the University of Clausthal by K. Hermann. We are grateful to him. We are also indepted to G. Hartmann and K. Simon (both of the Geochemisches Institut of the University of Göttingen) for XRF and ICP-MS analyses. The fluid inclusion study was supported by project GAČR 205/07/P130. We also acknowledge with thanks the reviews of the manuscript by K. Pošmourný, J. Zimák, the handling editor J. Cempírek and the editor-in-chief S. Houzar, whose critical comments and contributions led to a substantial improvement of the paper.

## REFERENCES


AHLBURG, J., 1911: Geologische Beziehungen zwischen den Eisenerzlagerstätten des Siegerlandes und des Lahn-Dillgebietes. – *Ztschr. prakt. Geol.* 19, 59–71.

AICHLER, J., FOJT, B., VANĚČEK, M., 1995: VIII.B.5 Metallogenesis. In: R.D. Dallmeyer, W. Franke, K. Weber (Eds): Pre-permian Geology of Central and Eastern Europe. – *Springer Verlag Berlin Heidelberg*, 512–517.

ANDERS, E., GREVESSE, N., 1989: Abundance of the elements: meteoric and solar. – *Geochim. Cosmochim. Acta* 53, 197–214.

BERDERKE, F., 1938: Die Eisenerzlagerstätten der Ostsudeten. – *Zt. Berg-, Hütten- und Salinenwesen* 86, 481–487.

BODNAR, R. J., BURNHAM, C. W., STERNER, S. M., 1985: Synthetic fluid inclusions in natural quartz. III. Determination of the phase equilibrium properties in the system $H_2O$-NaCl to 1 000 °C and 1 500 bars. – *Geochim. Cosmochim. Acta*, 49, 1 861–1 873.

BODNAR, R. J., 1993: Revised equation and table for determining the freezing point depression of $H_2O$-NaCl solutions. – *Geochim. Cosmochim. Acta*, 57, 683–684.

BOWERS, T. S., HELGESON, H. C., 1983: Calculation of the thermodynamic and geochemical consequences of nonideal mixing in the system $H_2O$-$CO_2$-NaCl on phase relations in geologic systems: equation of state for $H_2O$-$CO_2$-NaCl fluids at high pressures and temperatures. – *Geochim. Cosmochim. Acta*, 47, 1 247–1 275.

BROWN, PH. E., 1989: FLINCOR: A fluid inclusion data reduction and exploration program (abstr.). – *Second biennial Pan-American conference on research on fluid inclusions*, program with abstracts: 14.

CATHELINEAU, M., 1988: Cation site occupancy in chlorites and illites as a function of temperature. – *Clay Miner.* 23, 471–485.

CHAI, L., NAVROTZKY, A., 1996: Synthesis, characterization, and energetics of solid solutions along the dolomite-ankerite join, and implications for the stability of ordered $CaFe(CO_3)_2$. – *Am. Min.* 81, 1 141–1 147.

DAVIDSON, P. M., SYMMES, G. H., COHEN, B. A., REEDER, R. J., LINDSLEY, D. H., 1993: Synthesis of the new compound $CaFe(CO_3)_2$ and experimental constrains on the $(Ca,Fe)CO_3$ join. – *Geochim. Cosmochim. Acta* 57, 5 105–5 109.

FIŠERA, M., FEDIUKOVÁ, E., CHÁB, J., NOVOTNÝ, P., OPLETAL, M., 1982: Vysvětlivky k základní geologické mapě ČSR 1 : 25 000 14–244. – K. Studánka. – *MS*, Ústř. Úst. geol. Praha.

FLICK, H., BEHNISCH, R., 1990: Iron ore of the Lahn-Dill type formed by diagenetic seeping of pyroclastic sequences – a case study of the Schalstein section at Gänsberg (Weilburg). – *Geol. Rundsch.* 79, 401–415.

FLICK, H., LIPPERT, H. J., NESBOR, H. D., REQUADT, H., 1998: Lahn- und Dillmulde. – In: T. Kirnbauer (Ed): Geologie und hydrothermale Mineralisationen im rechtsrheinischen Schiefergebirge. – *Nassauischer Verein für Naturkunde*, Sonderband 1, 33–62.

FOJT, B., NOVOTNÝ, M., SEKANINA, J., ŠTELCL, J., 1961: Mineralogical characteristic of the geological map area (1 : 50 000) Jeseník (in Czech). – *Acta Mus. Sil.*, A 10, 19–33.

FOJT, B., HLADÍKOVÁ, J., KOPA, D., MOŠNA, P., 1993: Paragenesis of the magnetite-ore deposit under Malý Děd-Hill near Bělá pod Pradědem in the Jeseníky Mts (in Czech). – *Čas. Slez. Muz. (A)*, 153–174.

FOJT, B., VAVROŠOVÁ-KONEČNÁ, J., DOLNÍČEK, Z., 2007: Short characterization of the iron occurrence Skály near Rýmařov, Jeseníky Mts., Czech Republic (in Czech). – *Čas. Slez. Muz. (A)*, 1–22. Opava.

GOLDSMITH, J. R., GRAF, D. L., WITTERS, J., NORTHROP, D. A., 1962: Studies in the system $CaCO_3$-$MgCO_3$-$FeCO_3$: 1. Phase relations; 2. A method for major-element spectrochemical analysis; 3. Compositions of some ferroan dolomites. – *J. Geol.* 70, 659–688.

HEDENQUIST, J. W., HENLEY, R. W., 1985: The importance of $CO_2$ on freezing point measurements of fluid inclusions: evidence from active geothermal systems and implications for epithermal ore deposition. – *Econ. Geol.* 80, 1 379–1 406.

HEINRICH, H., HERRMANN, A. G., 1990: Praktikum der analytischen Geochemie. – *Springer Verlag Berlin Heidelberg*, pp 1–420.

HENTSCHEL, H., 1960: Zur Frage der Bildung der Eisenerze vom Lahn-Dill Typ. – *Freib. Forschungsh.* C79, 82–105.

HLADÍKOVÁ, J., KŘÍBEK, B., 1988: Distribution and isotopic composition of sulphidic sulphur in rocks of the north-eastern part of the Bohemian Massif. – *Čas. Mineral. Geol.* 33, 2, 113–129.

HOLLOWAY, J. R., 1981: Compositions and volumes of supercritical fluids in the earth's crust. – In: L.S. Hollister, M. L. Crawford (Eds): MAC Short Course in Fluid Inclusions, Vol. 6, pp. 13–38. Mineralogical Association of Canada.

HURAI, V., KIHLE, J., KOTULOVÁ, J., MARKO, F., ŚWIERCZEWSKA, A., 2002: Origin of methane in quartz crystals from the Tertiary accretionary wedge and fore-arc basin of the Western Carpathians. – *Appl. Geoch.* 17, 1 259–1 271.

Jowett, E. C., 1991: Fitting iron and magnesium into the hydrothermal chlorite geothermometer. – *GAC/MAC/SEG Joint Annual Meeting*, Toronto. Program with abstracts 16, A62.

Kalvoda, J., Bábek, O., Fatka, O., Leichmann, J., Melichar, R., Nehyba, S., Špaček, P., 2008: Brunovistulian terrane (Bohemian Massif, Central Europe) from late Proterozoic to late Paleozoic: a review. – *Int. J. Earth Sci.* (Geol. Rundsch.) 97: 497–518.

Kretschmer, F., 1906: Die Leptochlorite der mähr.-schles. Schalsteinformation. – *Centralblatt für Mineralogie* 10, 293 pp.

Kretschmer, F., 1917: Die erzführende Diabas- und Schalsteinzone Sternberg-Bennisch. – *Archiv für Lagerstättenforschung* 24, 1–198.

Kretschmer., F., 1918: Über die Eisensilikaterze des Diabas- und Schalsteinzuges Sternberg-Bennisch (Schlesien). – *N. Jb. Min.*, 19–42.

Leake, B. E.,Woolley, A. R., Arps, C. E. S., Birch, W. D., Gilbert, M. C., Grice, J. D., Hawthorne, F. C., Kato, A., Kisch, H. J., Krivovichev, V. G., Linthout, K., Liard, J., Mandarion, J., Maresch, W. V., Nickel, E. H., Rock, N. M. S., Schumacher, J. C., Smith, D. C., Ungaretti, L., Whittacker, E. J. W., Youzhi, G., 1997: Nomenclature of amphiboles. Report of the subcommittee on amphiboles of the international mineralogical association commission on new minerals and mineral names. – *Eur. J. Min.* 9, 623–642.

Lehmann, E., 1972: On the source of the iron in the Lahn ore deposits. – *Min. Dep.* 7, 247–270.

Liard, J., 1988: Chlorites: metamorphic petrology. – In: S.W. Bailey (Ed.): Hydrous Phyllosilicates. – *Review in Mineralogy* 19, 405–447.

Lippert, H. J., Flick, H., 1998: Vulkano-sedimentäre Roteisenerze vom Lahn-Dill-Typ. – In: T. Kirnbauer (Ed.): Geologie und hydrothermale Mineralisationen im rechtsrheinischen Schiefergebirge. – *Nassauischer Verein für Naturkunde*, Sonderband 1, 121–128.

Matthes, S., 1983: Mineralogie. Eine Einführung in die spezielle Mineralogie, Petrologie und Lagerstättenkunde. – *Springer-Verlag Berlin Heidelberg New York Tokyo*, 417 pp.

Melka, K., Vybíral, J., 1977: Geology of the iron deposits og the Upper Morava Valley and the mineralogy of the Fe-phyllosilicates. – *Journal of Geological Sciences*, economic geology, mineralogy, 18, 7–88. Praha. (in Czech)

Melka, K., 1965: Proposal of chlorite classification (in Czech). – *Věst. Ústř. úst. Geol.* 40, 23–29.

Mixa, P., Orel, P., 1990: Evidence of submarine geothermal Paleozoic activity in the eastern part of Middle European Variscides (Czechoslovakia). – *8th IAGOD symp.*, Program with abstr. A 95, Geological Survey of Canada, Ottawa.

Mücke, A., Losos, Z., 2007: The magnetite mineralizations of the Desná Group in the Silesicum, Czech Republic: petrographic, mineralogical, and geochemical studies and their genetic implications. – *J. Geosciences* 52, 227–270.

Mücke, A., 2003: General and comparative considerations of whole-rock and mineral compositions of Precambrian iron-formations and their implications. – *N. Jb. Miner. Abh.* 179, 175–219.

Mücke, A. 2006: Chamosite, siderite and the environmental conditions of their formation in chamosite-type Phanerozoic ooidal ironstones. – *Ore Geol. Rev.* 28, 235–249.

Nesbor, H. D., Flick, H., 1988: Das Schalsteinprofil vom Gänsberg bei Weilburg. Aufbau und fazielle Entwicklung einer submarinen pyroklastischen Abfolge in Devon der Lahnmulde (Rheinisches Schiefergebirge). – *Geol. Jb. Hessen* 116, 189–205.

Petránek, J., 1976: Sedimentary iron ores of the Lahn-Dill type: a new concept of their origin. – *Věst. Ústř. Úst. geol.* 51, 203–207.

Pouba, Z., Hettler, J., 1950: Report about iron ores in the middle part of the High Jeseníky Mountains (in Czech). – *Geol. Surv. Prague*, 16 pp.

Pouba, Z., 1970: Pre-Cambrian banded magnetite ores of the Desná Dome. – *Sbor. Geol. Věd*, ložisk Geol. Mineral. 12, 7–170.

Pouba, Z., 1971: Relations between iron and copper-lead-zinc mineralizations in submarine volcanic ore deposits in the Jeseníky Mts., Czechoslovakia. – *Soc. Mining Geol.*, Japan, Special Issue 3, 186–192.

Pouchou, J. L., Pichoir, F., 1984: A new model for quantitative X-ray microanalysis. Part I: Application to the analysis of homogenous samples. – *Rechérches Aérospatiale* 3: 13–38

Quade, H., 1976: Genetic problems and environmental features of volcano-sedimentary iron ore deposits of the Lahn-Dill type. In: K.H. Wolfe (Ed.): Handbook of strata-bound and stratiform ore deposits. – *Elsevier Amsterdam*, 255–294.

Reeder, R. J., Dollase. W. A., 1989: Structural variation in the dolomite-ankerite solid-solution series: An X-ray, Mössbauer, and TEM study. – *Am. Min.* 74, 1 159–1 167.

Reeder, R. J., Dollase, W. A., 1991: Structural variation in the dolomite-ankerite solid-solution series: An X-ray, mössbauer, and TEM study – Reply. – *Am. Min.* 74, 661–662.

Reeder, R. J., 1983: Crystal chemistry of rhombohedral carbonates. In: R. J. Reeder (Ed.): Carbonates: Mineralogy and chemistry. – *Review in Mineralogy* 11, Min. Soc. Am., 1–47.

Rieder, M., Cavazzini, G. D., Yakonov, Y., Gottardi, G., Guggenheim, S., Koval, P. V., Müller, G., Neiva, A. M. R., Radoslovich, E. W., Robert, J. L., Sassi, F. P., Takeda, H., Weiss, Z., Wones, D. R., 1998: Nomenclature of the micas. – *Can. Mineral.* 36, 905–912.

Roedder, E., 1984: Fluid inclusions. – *Rev. Mineral.* 12, 1–644.

Rosenberg, P. E., 1963: Subsolidus relations in the system $CaCO_3$ – $FeCO_3$. – *Am. J. Sc.* 261, 683–690

Rosenberg, P. E., 1967: Subsolidus relations in the system $CaCO_3$-$MgCO_3$-$FeCO_3$ between 350 and 550 °C. – *Am. Min.* 52, 787–796.

Rosenberg, P. E., 1991: Structural variation in the dolomite-ankerite solid-solution series: An X-ray, mössbauer, and TEM study - Discussion. – *Am. Min.* 76, 659–660.

Rösler, H. J., 1964: Genetische Probleme der Erze des sogenannten erweiterten Lahn-Dill Typus. – *Ber. Geol. Ges. DDR* 9, 445–454.

Sawkins, F. J., Burke, K., 1980: Extensional tectonics and mid-Paleozoic massive sulfide occurrences in Europe. – *Geol. Rund.* 69, 349–360.

Sawkins, F. J., 1990: Metal deposits in relation to plate tectonics, second edition. – *Springer Verlag Berlin Heidelberg New York*, 461pp.

Sawlowicz, Z., 1989: On the origin of copper mineralization in the Kupferschiefer: a sulfur isotope study. – *Terra Nova* 1, 339–343.

Schulmann, K., Gayer, R., 2000: A model for a continental accretionary wedge by oblique collision. – *J. Geol. Soc.*, London 157; 401–416.

Schumacher, J. C., 1997: The estimation of ferric iron in electron microprobe analysis of amphiboles. – *Eur. J. Min.* 9, 643–651.

Sellner, F., 1930: Die Magnetitlagerstätten der tschechoslowakischen Republik. III. Die Vorkommen im Altvatergebirge bei Leiterberg. – *Zt. angew. Geol.* 38, 179–189.

Shepherd, T. J., Rankin, A. H., Alderton, D. H. M., 1985: A practical guide to fluid inclusion studies. Blackie, Glasgow and London.

Sheppard, S. M. F., 1986: Characterization and isotopic variations in natural waters. – *Rev. Mineral.* 16, 165–183.

Skácel, J., 1966: Die Eisenerzlagerstätten des Mährisch-Schlesischen Devons (in Czech). – *Rozpr. ČSAV*, řada. matematických a přírodních Věd. 76, 3–61.

Skácel, J., 1987: The Silesikum and adjacent parts of the Lugicum: ore deposits and metallogeny. – *Geol. Surv. Prague*, Excursion guide for inaugural Meeting of JGCP Project 245, 15–23.

Thiéry, R., van den Kerkhof, A. M., Dubessy, J., 1994: VX properties of $CH_4$-$CO_2$ and $CO_2$-$N_2$ fluid inclusions: modelling for T <31°C and P <400 bars. – *Eur. J. Min.* 6, 6, 753–771.

Touret, J. L. R., 2001: Fluids in metamorphic rocks. – *Lithos* 55, 1–25.

van den Kerkhof, F., Thiéry, R., 1994: Phase transitions and density calculation in the $CO_2$-$CH_4$-$N_2$ system. In: B. De Vivo, M.L. Frezotti (Eds.): Fluid inclusion in minerals: methods and applications, pp 171–190. – *Virginia Tech*, Blacksburg.

Wilschowitz, J., 1929: Das neue Magnetitvorkommen am Leiterberg bei Waldenburg in Schlesien. – *Mitt. Naturwis*. Ver. Troppau (ČSR) 35, 3–11.

Žáček, V., 2007: Minerals of metamorphosed iron deposit of Seč at Jeseník, Silesicum, Czech Republic. – *Bull. mineral-petrol. odd.*, Nár. Muz. Praha 14/15, 198–200. Praha.

Zhang, Y. G., Frantz, J. D., 1987: Determination of the homogenization temperatures and densities of supercritical fluids in the system NaCl-KCl-$CaCl_2$-$H_2O$ using synthetic fluid inclusions. – *Chem. Geol.* 64, 335–350.

Zimák, J., Vávra, V., 1998: Monazite in silicate Fe-ores of the Lahn-Dill type near Chabičov (in Czech). – *Geol. Výzk. Mor. Slez. v r 1997*, 5, 72–73, Brno.

Zimák, J., 2000: Mineralogy of iron ores of the Lahn-Dill type at the locality "Drakov" near Heřmanovice (in Czech). – *Geol. Výzk. Mor. Slez. v roce 1999, 7*, 108–110. Brno.

Zimák, J., 2001: Mineralogy of iron ores of the Lahn-Dill type at the locality "Maria Trost" (Tvrdkovská Leč) near Heřmanovice (in Czech). – *Geol. Výzk. Mor. Slez. v r. 2000*, 8, 63–65. Brno.

Zimák, J., 2002a: Calcite marble with magnetite at the locality "Mlýnský vrch" near Heřmanovice (in Czech). – *Geol. Výzk. Mor. Slez. v r. 2001*, 65–67. Brno.

Zimák, J., 2002b: Mineralogy of iron ores at the historical deposit „Glück Auf" near Seč (near Jeseník) (in Czech). – *Geol. Výzk. Mor. Slez. v r. 2001*, 82–84. Brno.